Zic gene function, the exact role these genes play *in vivo* has yet to be elucidated. *In vitro*, ZIC2 inhibits WNT/β-catenin signaling through a direct interaction with TCF4 (Pourebrahim, Houtmeyers et al. 2011) and ZIC proteins interact with GLI transcription factors to either suppress or enhance GLI-mediated transactivation (Koyabu, Nakata et al. 2001; Mizugishi, Aruga et al. 2001; Pan, Gustafsson et al. 2011). In *Xenopus*, *Zic* genes both activate and inhibit WNT/β-catenin signaling (Merzdorf and Sive 2006; Pourebrahim, Houtmeyers et al. 2011; Fujimi, Hatayama et al. 2012), and in zebrafish, *Zic* genes regulate expression of *shh* and *nodal* and modulate Hedgehog-mediated gene expression (Maurus and Harris 2009; Sanek, Taylor et al. 2009).

Given the importance of *Zic* gene expression in the neural tube, as well as the ability of *Zic* genes to modulate WNT and SHH signaling, key pathways known to be involved in dorso-ventral patterning of the inner ear (Riccomagno, Martinu et al. 2002; Riccomagno, Takada et al. 2005), surprisingly little attention has been paid to *Zic* gene expression and function in and around the developing inner ear. One early study identified *Zic2* as one of the first genes up-regulated in the regenerating sensory epithelium of the chicken inner ear after noise exposure (Gong, Hegeman et al. 1996). Conflicting data exist regarding the location of *Zic* gene expression during inner ear development (Warner, Hutson et al. 2003; McMahon and Merzdorf 2010). Although some *Zic* expression patterns have been described in the mouse (reviewed in Merzdorf 2007; Ali, Bellchambers et al. 2012), to date *Zic* expression in the developing mouse inner ear has not been examined. Given the discrepancies in the *Zic* gene expression patterns

described in the earlier studies, we have undertaken a more extensive comparative spatiotemporal analysis of *Zic* mRNA expression in the otic regions of both the chick and mouse during the early stages of inner ear development.

2.3. Results

Evolutionary Conservation of the *Zic* Genes Across Species

Phylogenetic analysis of ZIC proteins from mouse (ZIC1-5), human (ZIC1-5), chicken (ZIC1-4), zebrafish (Zic1/Opl, Zic1-like, Zic2a and b, and Zic3-6), frog (Zic1, Zic2a and 2b, and Zic3-5), and fly (Odd-paired; OPA) indicate significant conservation among species (Fig. 2-1A). ZIC proteins from across species clustered together into five groups, with each representing one of the 5 *Zic* genes. In addition to these 5 clusters, Zic6 and Zic1-like from zebrafish grouped together with the ancestral protein from the fly, odd-paired, into a 6^{th} cluster. The ZIC1, ZIC2, and ZIC3 clusters group together, the ZIC5 and odd-paired clusters group together, and the ZIC4 proteins form two groups (mouse/human, and chick/frog/fish) that cluster together away from all of the other Zics. Within each of the five major clusters (ZIC1-5), the mouse and human genes are closely related to one another, and more distantly related to those from chicken, zebrafish, and frog.

Identity and similarity comparisons among the complete amino acid sequences of the mouse, human, and chicken ZIC proteins indicates that the mouse and human ZIC1, ZIC2, and ZIC3 proteins are almost identical, but the ZIC4 and ZIC5 proteins differ slightly (Fig. 2-1B). Chicken Zic1 is very similar to

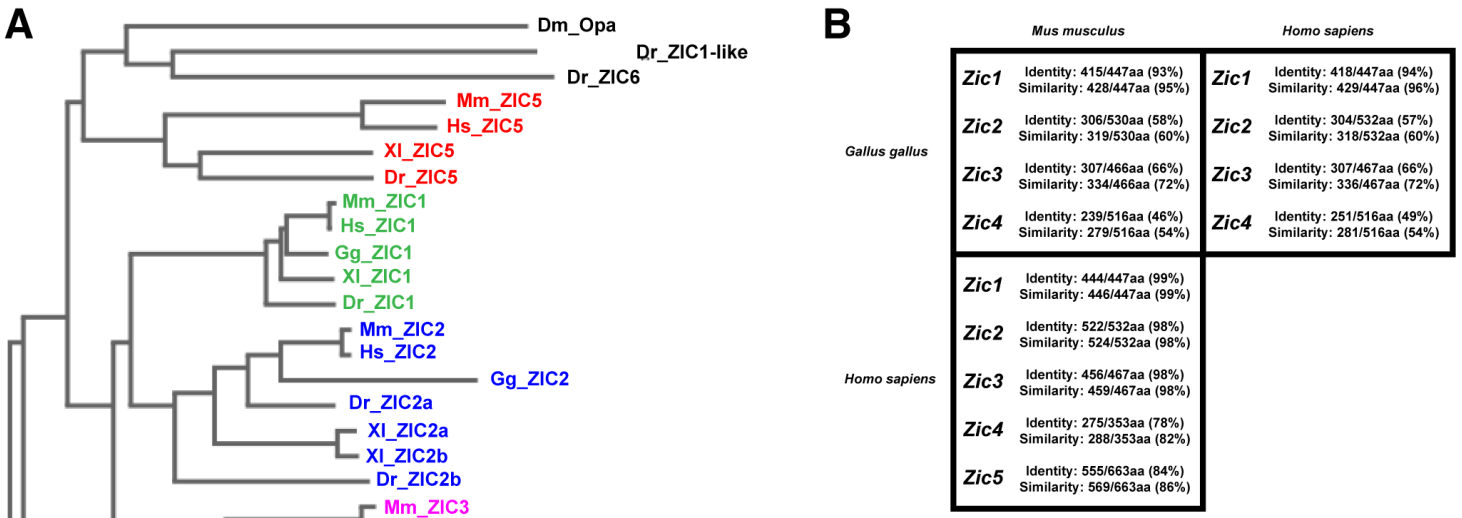

Figure 2-1. Comparison of *Zic* Genes Across Species. (A) Phylogenetic tree showing the relationships among the *Zic* genes from human, mouse, chick, zebrafish, and frog, as well as the ancestral gene *odd-paired* (*opa*) from *Drosophila*. The complete amino acid sequences were used for the construction of the tree. (B) Percent identity and similarity of the amino acid sequences among the mouse, chick, and human ZIC proteins. The chick ZIC2, ZIC3, and ZIC4 protein sequences have not been finalized, so comparisons to these protein sequences result in much lower percent identity and similarity. Abbreviations: Dm, *Drosophila melanogaster*; Dr, *Danio rerio*; Gg, *Gallus gallus*; Hs, *Homo sapiens*; Mm, *Mus musculus*; Xl, *Xenopus laevis*

both mouse and human ZIC1 proteins, but chicken Zic2-Zic4 differ greatly from mouse and human ZIC2-4, with Zic4 being the most different. Zic1-3 are the most similar between chicken and mouse and human, while Zic4 is not as conserved. ZIC1-3 contain a Zic-opa conserved (ZOC) domain, resulting in a higher level of homology among these proteins, while ZIC4 and ZIC5 do not. The ZOC domain is required for activation of target gene transcription *in vitro*, as well as for binding I-mfa, a myogenic repressor protein (Mizugishi, Hatayama et al. 2004). Further, the intron-exon boundaries are conserved between ZIC1-3, but not between ZIC1-3 and either ZIC4 or ZIC5 (Grinberg and Millen 2005). This suggests that the *Zic4* and *Zic5* genes are the most divergent and may have evolved novel functions. ZIC1 is almost identical in mouse, human, and chicken and therefore may have the same function in all three organisms. ZIC2 and ZIC3 are almost identical between mouse and human, but differ when compared to chick Zic2 and Zic3, suggesting that they may have different functions in birds and mammals.

Comparison of otic development in chick and mouse

The early stages of inner ear development are similar in both the chick and in the mouse (summarized in Fig. 2-2), and require signaling from different tissues to specify and pattern the otic placode (underlying mesoderm), otocyst (mesenchyme, neural tube, notochord), and inner ear (mesenchyme, neural tube, notochord). Initially, cells in the dorsal ectoderm adjacent to rhombomeres 5 and 6 of the hindbrain thicken, forming the otic placode (HH stage 10 in chick

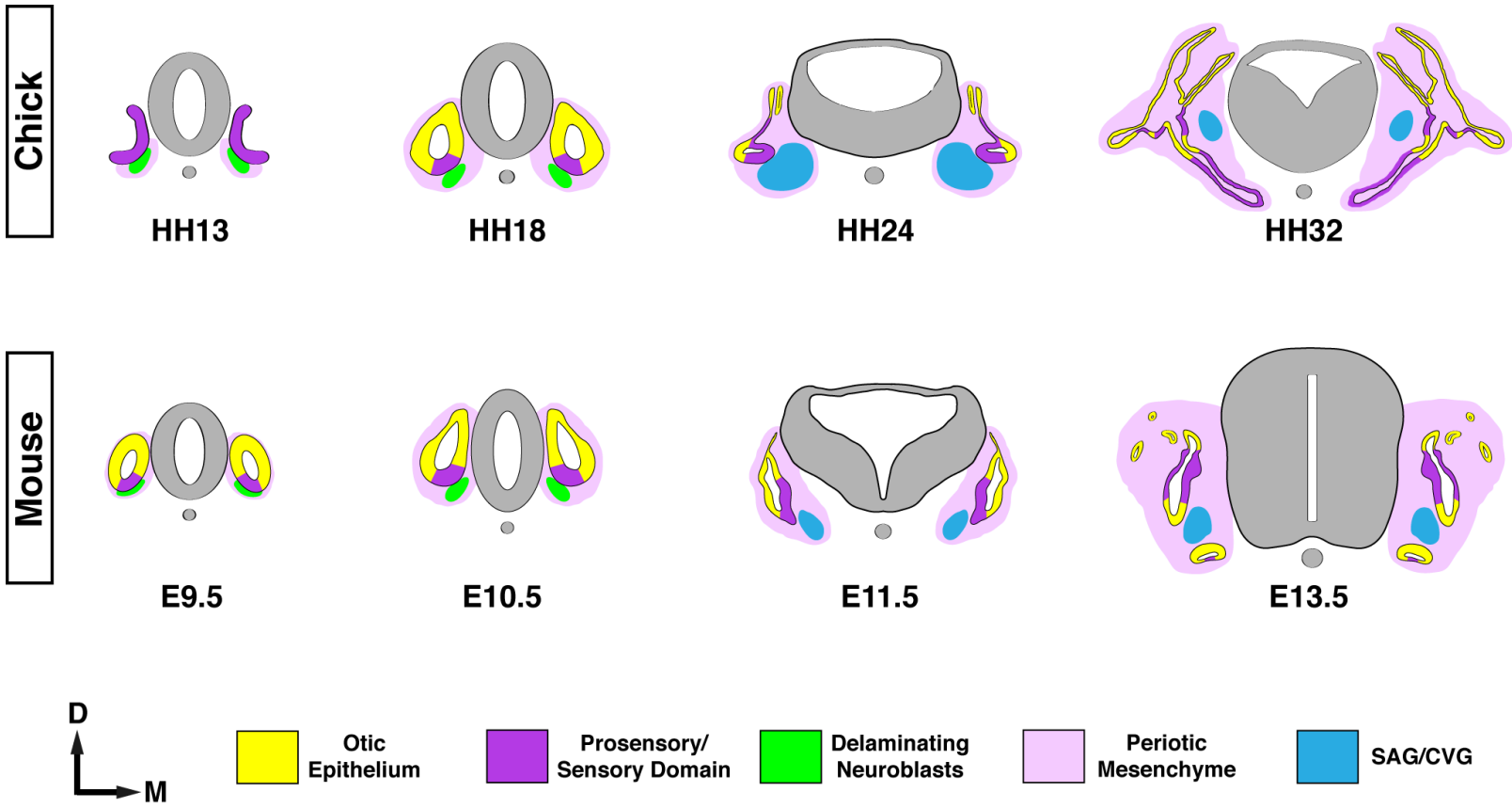

Figure 2-2. Inner Ear Development in Chicken and Mouse. Schematic depicting inner ear development in chicken from stage 13 to stage 32 (top row) and in mouse from E9.5 to E13.5 (lower row). Gray shaded regions correspond to the neural tube and the notochord. Images are based upon transverse sections through the middle of the otocyst, but are not to scale. Abbreviations: sag, statoacoustic ganglion; cvg, cochleovestibular ganglion; d, dorsal; m, medial.

(Hamburger and Hamilton 1992), embryonic day 8 to 8.5 (E8-E8.5) in mouse). Subsequently, the placode invaginates to form the otic cup, and neuroblasts begin to delaminate from the ventral region of the otic cup and migrate away to form the cochleovestibular ganglion (CVG)/statoacoustic ganglion (SAG) (HH stage 13 in chick, E8.75-E9 in mouse). The otic cup closes completely and pinches off from the overlying ectoderm, forming the otic vesicle/otocyst (HH stage 17 in chick, E9.5 in mouse). Over the next several days the otocyst undergoes complex morphological changes, transforming into a complex structure comprised of three semicircular canals, the utricle, the saccule, and the cochlea (mouse)/basilar papilla (chick).

Expression of the *Zic* genes during otic development in chick and mouse

We used *in situ* hybridization to examine the expression of the *Zic* genes (*Zic1-4* in chick, *Zic1-5* in mouse; refer to Fig. 2-3 for the location of the riboprobes within each gene) in the hindbrain and in the adjacent region of the developing inner ear in the chick (HH stage 13 to HH stage 32) and in the mouse (E9.5 to E13.5). *Pax2* expression in this region, which has previously been reported for both chick (Hutson, Lewis et al. 1999; Hidalgo-Sanchez, Alvarado-Mallart et al. 2000; Sanchez-Calderon, Martin-Partido et al. 2002; Li, Liu et al. 2004; Sanchez-Calderon, Martin-Partido et al. 2005) and mouse (Nornes, Dressler et al. 1990; Puschel, Westerfield et al. 1992; Rinkwitz-Brandt, Justus et al. 1995; Rinkwitz-Brandt, Arnold et al. 1996; Lawoko-Kerali, Rivolta et al. 2002; Burton, Cole et al. 2004), is included in the same series of *in situ* hybridizations as an internal

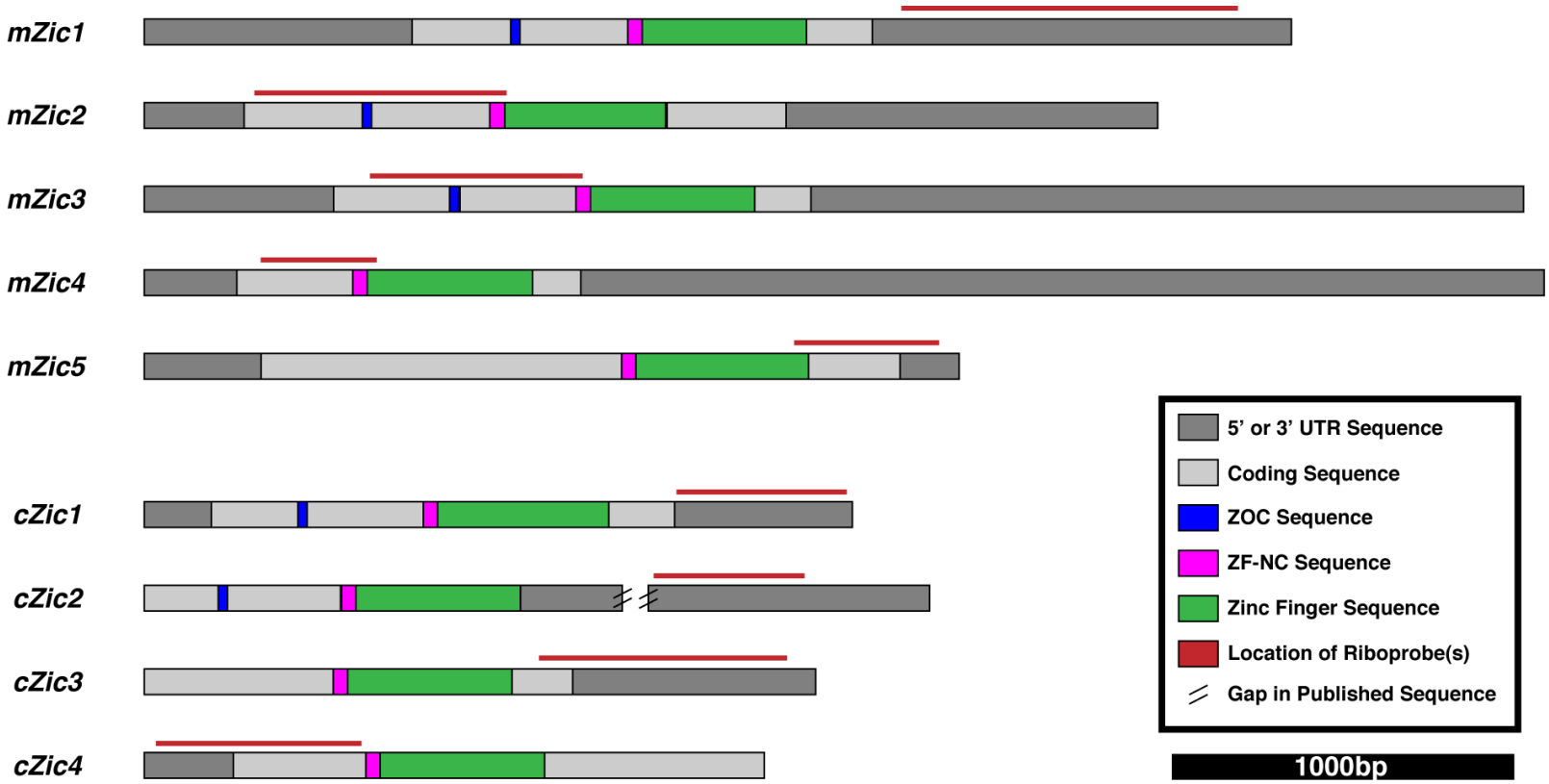

Figure 2-3. Location of Riboprobes Within the mRNA Sequence of the *Zic* Genes. Diagrams of the mRNA sequence for each *Zic* gene illustrate the location of the coding sequence (light gray boxes), UTRs (dark gray boxes), and functional domains (blue, magenta, and green boxes) within each of the *Zic* genes. Probes for each of the *Zic* genes in mouse (*Zic1-5*) and chick (*Zic1-4*) were designed to target the less-conserved 5' and 3' UTR regions of each gene (red lines above the mRNA diagram show the location of the riboprobes). The published sequences for chick *Zic2-4* are still being annotated and updated, so the most 5' and 3' untranslated regions of the mRNA have not been defined. Abbreviations: UTR, untranslated region; ZOC, Zic-opa conserved domain; ZF-NC, zinc-finger nucleocapsid domain.

control for otic epithelial gene expression.

Expression of *Zic* genes in the developing chick inner ear

At HH stage 13, *Pax2* was expressed throughout the epithelium of the otic cup but not in the adjacent neuroepithelium of the developing neural tube (Fig. 2-4A). By HH stage 18, the otic cup has closed to form the otocyst (Fig. 2-2, top row) and *Pax2* expression was restricted to the medial and ventral walls of the otic epithelium (Fig. 2-4F). At this stage, *Pax2* expression was also detected in the ventral neural tube. Between HH stages 18 and 24, the spherical otocyst elongates to form the early inner ear with identifiable dorsal (endolymphatic duct and sac) and ventral (basilar papilla) structures (top row, Fig. 2-2). *Pax2* expression at HH stage 24 (Fig. 2-4K) was further restricted to the endolymphatic duct and prosensory regions of the otic epithelium, and was maintained in the ventral neural tube. In contrast to *Pax2*, expression of the *Zic* genes was not detected in the otic epithelium at HH stages 13, 18, or 24 (Fig. 2-4). Expression of *Zic1-3* was detected in the dorsal neural tube at HH stages 13, 18, and 24, but *Zic4* expression was not detected in the dorsal neural tube until HH stages 18 (weak) and 24 (asterisks in Fig. 2-4B, 2-4C, 2-4D, 2-4G, 2-4H, 2-4I, 2-4J, 2-4L, 2-4M, 2-4N, 2-4O). Following otocyst closure at HH stage 18, *Zic1-3* expression was observed laterally around the outside of the otocyst (black arrowheads, Fig. 2-4G, 2-4H, 2-4I), and *Zic1* and *Zic2* expression was detected medially between the otic epithelium and the neural tube (yellow arrows, Fig. 2-4G, 2-4H). By HH stage 24, expression of *Zic1-4* was observed medially between the developing

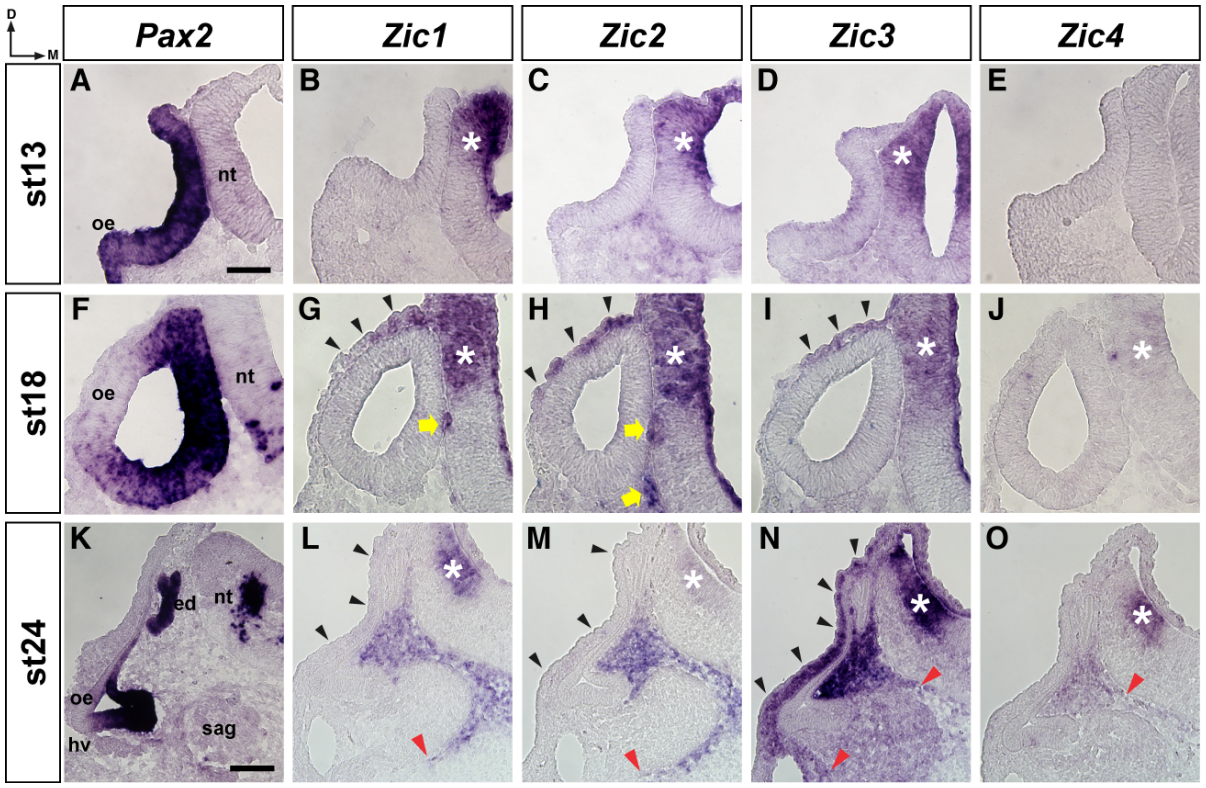

Figure 2-4. *Zic* Expression in the Otic Region of Early Stage Chick Embryos. *In situ* hybridization on 12μm transverse sections through the otocyst of stage 13 (A-E), stage 18 (F-J), and stage 24 (K-O) chick embryos using probes for *Pax2* (A, F, K), *Zic1* (B, G, L), *Zic2* (C, H, M), *Zic3* (D, I, N), and *Zic4* (E, J, O). Note that *Pax2* is expressed in sensory regions of the otic epithelium, while *Zic* gene expression is restricted to the surrounding mesenchyme. Abbreviations: oe, otic epithelium; ed, endolymphatic duct; nt, neural tube; sag, statoacoustic ganglion; hv, head vein; d, dorsal; m, medial. Asterisks identify *Zic* expression in the neural tube (B, C, D, G, H, I, J, L, M, N, O). Black arrowheads indicate *Zic*-expressing cells between the outer epithelium and the otic epithelium (G, H, I, L, M, N). Yellow arrow indicates *Zic*-expressing cells between neural tube and otic epithelium (G, H). Red arrowheads indicate the ventral-most extent of *Zic* expression in the mesenchyme (L, M, N, O). Scale bar in A, 50μm (applies to A-J); scale bar in K, 100μm (applies to K-O).

inner ear and the neural tube, with the ventral extent of expression varying among the *Zic* genes (Fig. 2-4L, 2-4M, 2-4N, 2-4O; the red arrowheads indicates ventral extent of *Zic*-expressing cells). Weak *Zic1* and *Zic2* expression, as well as strong *Zic3* expression, was observed lateral to the developing inner ear (black arrowheads, Fig. 2-4L, 2-4M, 2-4N).

Between HH stages 24 and 32, the developing inner ear has undergone further morphological changes, resulting in an inner ear with clearly defined structures with identifiable prosensory domains (Fig. 2-2, top row; Fig. 2-5). *Pax2* was expressed in the endolymphatic duct and the neuroepithelium of the neural tube (Fig. 2-5A; blue dashed line marks border between otic epithelium and the surrounding mesenchyme) and in the emerging sensory patches within the otic epithelium of the basilar papilla (Fig. 2-5F), the crista of the lateral semicircular canal (asterisk, Fig. 2-5K), the utricular macula (arrowheads, Fig. 2-5P), and the saccular macula (blue arrows, Fig. 2-5P). *Zic1-4* expression was not detected in the otic epithelium at HH stage 32 (Fig. 2-5). However, *Zic1-4* expression was detected in the dorsal neural tube and adjacent to the otic epithelium (Fig. 2-5B, 2-5C, 2-5D, 2-5E; a blue dashed line in Fig. 2-5B marks the border between the otic epithelium and the surrounding mesenchyme). *Zic2* was the only *Zic* gene expressed surrounding the entire otic epithelium, including the developing basilar papilla (Fig. 2-5H), lateral semicircular canal (Fig. 2-5M), and the utricular and saccular maculae (Fig. 2-5R). Expression of the other *Zic* genes was restricted to the mesenchyme adjacent to specific regions of the otic epithelium. *Zic1* expression was limited to the dorsomedial region of the mesenchyme between

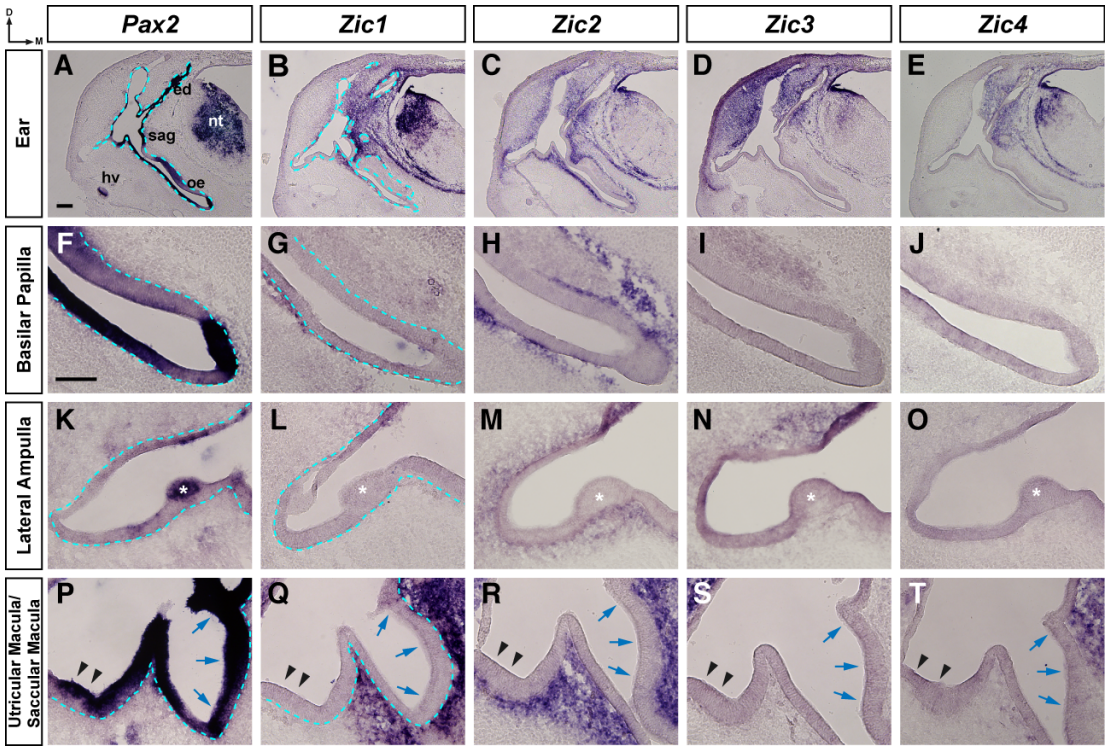

Figure 2-5. *Zic* Expression in the Otic Region of Stage 32 Chick Embryos. *In situ* hybridization on 25μm transverse sections through the otocyst of stage 32 chick embryos using probes for *Pax2* (A, F, K, P), *Zic1* (B, G, L, Q), *Zic2* (C, H, M, R), *Zic3* (D, I, N, S), and *Zic4* (E, J, O, T). Expression at low magnification in the ear (A-E), and at higher magnification in the basilar papilla (F-J), Lateral ampulla (K-O) and utricular/saccular maculae (P-T). Note that *Pax2* is expressed in sensory regions of the otic epithelium, while *Zic* gene expression is restricted to the surrounding mesenchyme. In panels 5L-5N, the otic epithelium at the upper right corner is darkened as a result of tissue folding. Abbreviations: oe, otic epithelium; ed, endolymphatic duct; nt, neural tube; gl, ganglion; hv, head vein; d, dorsal; m, medial. Asterisks identify the lateral ampulla (K, L, M, N, O). Black arrowheads indicate the utricular macula and blue arrows denote the saccular macula (P, Q, R, S, T). Blue dashed line defines border between the otic epithelium and the mesenchyme (first two columns). Scale bar in A, 200μm (applies to A-E); scale bar in F, 100μm (applies to F-T).

the otic epithelium and neural tube, but was also detected adjacent to a portion of the ventral basilar papilla (Fig. 2-5G), next to the dorsolateral wall of the ear (Fig. 2-5L), and surrounding the saccular macula but not the utricular macula (Fig. 2-5Q). *Zic3* expression was restricted to cells surrounding the dorsal region of the developing inner ear, including cells adjacent to the dorsal wall of the lateral semicircular canal (Fig. 2-5N), but was not found in cells adjacent to the basilar papilla (Fig. 2-5I) or the utricular and saccular maculae (Fig. 2-5S). *Zic4* had the most restricted expression pattern, expressed in the mesenchyme in the dorsomedial region between the otic epithelium and neural tube, including in cells adjacent to the dorsomedial portion of the saccular macula (Fig. 2-5T), but not in cells adjacent to the basilar papilla (Fig. 2-5J) or in cells adjacent to the lateral semicircular canal (Fig. 2-5O).

Expression of *Zic* genes in the developing mouse inner ear

At E9.5, *Pax2* was expressed in ventromedial wall of the otocyst but not in the adjacent neuroepithelium of the developing neural tube of the mouse (Fig. 2-6A). By E10.5, the otocyst has begun to elongate (Fig. 2-2, bottom row) and *Pax2* expression remained in the lateral and ventromedial wall of the otocyst (Fig. 2-6G). Between E10.5 and E11.5, the otocyst undergoes further morphological changes, elongating along its dorso-ventral axis and becoming compacted along its medio-lateral axis, forming the endolymphatic duct at the dorsal end and the start of the cochlear duct at the ventral end (Fig. 2-2, bottom row). At E11.5, *Pax2* was expressed in the neural tube, in the endolymphatic duct, and in the

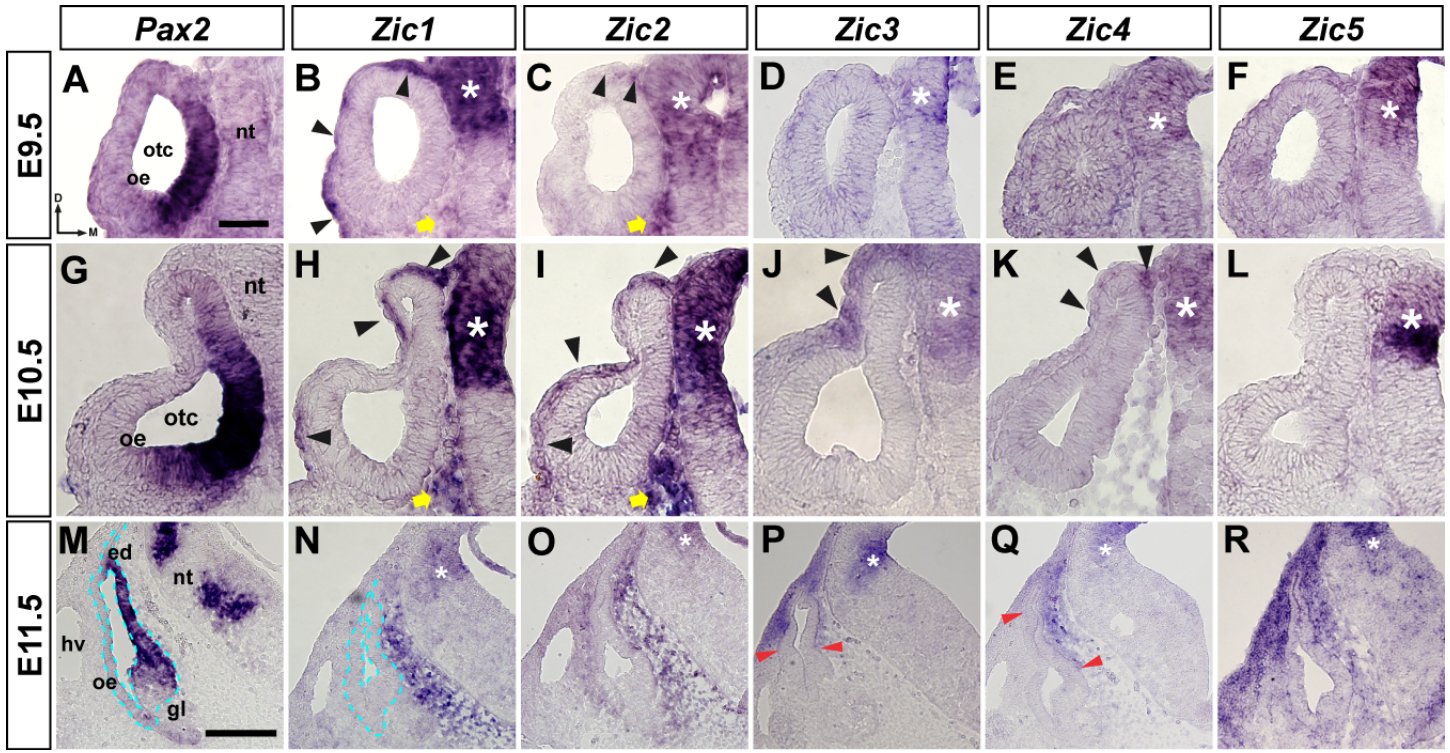

Figure 2-6. *Zic* Expression in the Otic Region of Mouse Embryos Between E9.5 and E11.5. *In situ* hybridization on 12μm transverse sections through the otocyst of E9.5 (A-F), E10.5 (G-L), and E11.5 (M-R) mouse embryos using probes for *Pax2* (A, G, M), *Zic1* (B, H, N), *Zic2* (C, I, O), *Zic3* (D, J, P), *Zic4* (E, K, Q), and *Zic5* (F, L, R). Note that *Pax2* is expressed in the otic epithelium, while *Zic* gene expression is restricted to the surrounding mesenchyme. Abbreviations: otc, otocyst; oe, otic epithelium; nt, neural tube; ed, endolymphatic duct; gl, ganglion; hv, head vein; d, dorsal; m, medial. Asterisks identify *Zic* expression in the neural tube (B-F, H-L, N-R). Black arrowheads indicate *Zic*-expressing cells between the surface ectoderm and the otic epithelium (B, C, H, I, J, K). Yellow arrows indicate *Zic*-expressing cells between neural tube and otic epithelium (B, C, H, I). Red arrowheads indicate the ventral-most extent of *Zic* expression in the mesenchyme (P, Q). Blue dashed line defines border between the otic epithelium and the mesenchyme (M, N). Scale bar in A, 50μm (applies to A-L); scale bar in M, 200μm (applies to M-R).

developing sensory patches of the otic epithelium, but not in the mesenchyme surrounding the developing inner ear (Fig. 2-6M; a blue dashed line marks the border between the otic epithelium and the surrounding mesenchyme). In contrast to *Pax2*, expression of *Zic1-5* was not detected in the otic epithelium at E9.5, E10.5, or E11.5 (Fig. 2-6). *Zic1-5* expression was seen in the dorsal neural tube at E9.5, E10.5, and E11.5 (asterisks in Fig. 2-6B to 2-6F, 2-6H to 2-6L, 2-6N to 2-6R). *Zic1*- and *Zic2*-expressing cells were found in the mesenchyme between the ventral neural tube and the otic epithelium and adjacent to the dorsolateral side of the otocyst at E9.5 and E10.5, although the *Zic2*-expressing cells were not seen as far ventrally as were the *Zic1*-expressing cells (yellow arrow and black arrowheads, Fig. 2-6B, 2-6C, 2-6H, 2-6I). *Zic3*- and *Zic4*-expressing cells were also found adjacent to the dorsolateral side of the otocyst at E10.5 (black arrowheads, Fig. 2-6J, 2-6K). By E11.5, *Zic1* expression was seen in cells located medially between the otic epithelium and the neural tube (Fig. 2-6N; a blue dashed line marks the border between otic epithelium and the surrounding mesenchyme), while *Zic2*- and *Zic5*-expressing cells surrounded the entire otic epithelium, although Zic5 was expressed more strongly adjacent to the dorsal region of the otic epithelium (Fig. 2-6O, 2-6R). *Zic3* and *Zic4* expression was restricted to the mesenchyme surrounding the dorsal half of the otic epithelium, with *Zic3* expression extending further ventrally than *Zic4* on the lateral side of the otic epithelium and *Zic4* expression extending further ventrally than *Zic3* on the medial side of the otic epithelium (Fig. 2-6P, 2-6Q; red arrowheads denote the ventral extent of expression).

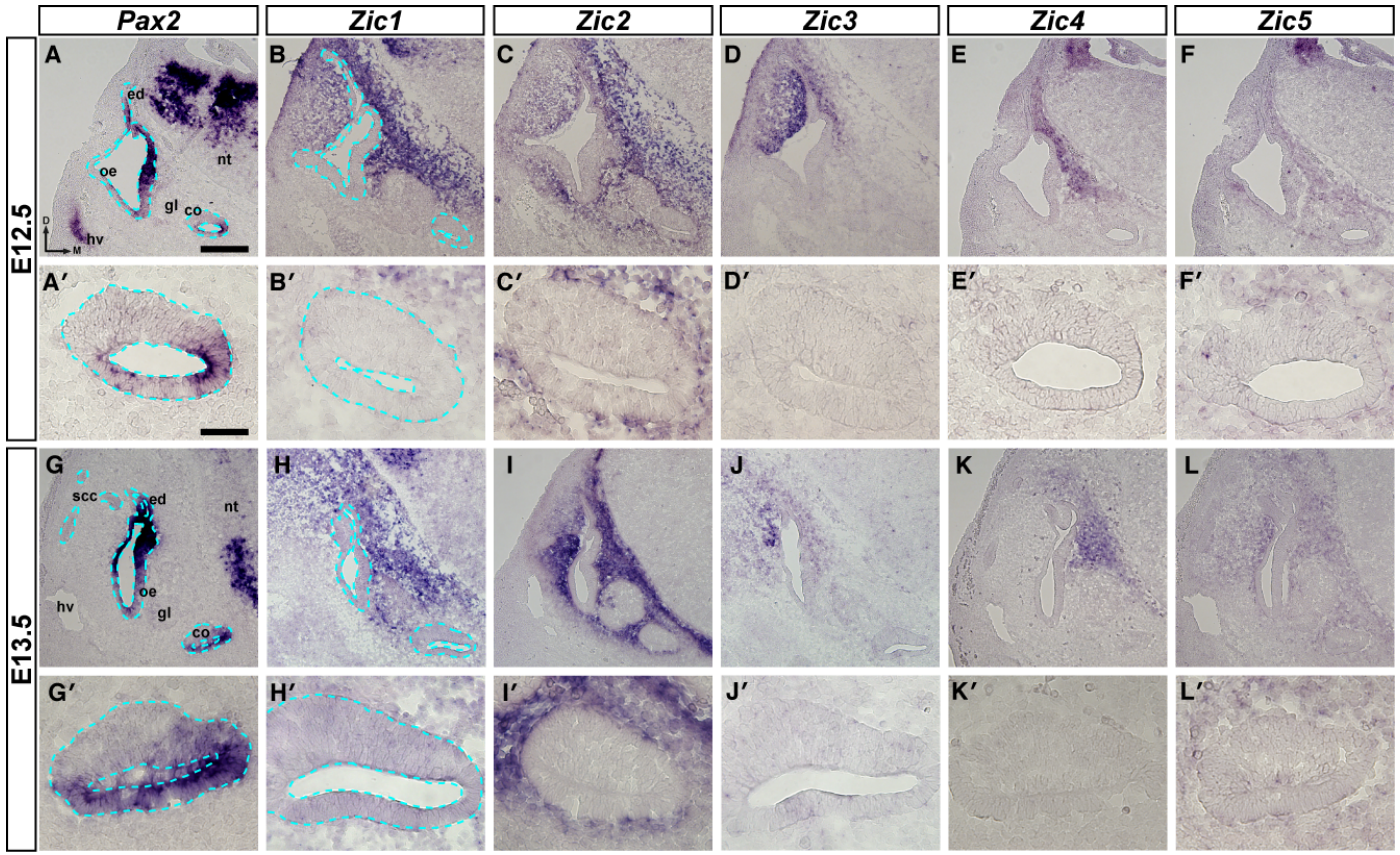

Figure 2-7. *Zic* Expression in the Otic Region of E12.5 and E13.5 Mouse Embryos. *In situ* hybridization on 12μm transverse sections through the otocyst of E12.5 (A-F, A'-F') and E13.5 (G-L, G'-L') mouse embryos using probes for *Pax2* (A, A', G, G'), *Zic1* (B, B', H, H'), *Zic2* (C, C', I, I'), *Zic3* (D, D', J, J'), *Zic4* (E, E', K, K'), and *Zic5* (F, F', L, L'). Note that *Pax2* is expressed in the otic epithelium, while *Zic* gene expression is restricted to the surrounding mesenchyme. Abbreviations: oe, otic epithelium; ed, endolymphatic duct; co, cochlea; scc, semicircular canals; nt, neural tube; gl, ganglion; hv, head vein; d, dorsal; m, medial. Blue dashed line defines border between the otic epithelium and the mesenchyme (A, A', B, B', G, G', H, H'). Scale bar in A, 200μm (applies to A-L); scale bar in A', 50μm (applies to A'-L').

At E12.5 and E13.5, *Pax2* was expressed in the neural tube, endolymphatic duct, and the developing sensory patches of the otic epithelium (Fig. 2-7A, 2-7G; a blue dashed line marks the border between the otic epithelium and the surrounding mesenchyme), including the developing cochlear duct (Fig. 2-7A', 2-7G'), but was not found in the mesenchyme surrounding the developing inner ear. *Zic1-5* were expressed in the dorsal neural tube (data not shown), but in contrast to *Pax2*, they were not expressed in the otic epithelium (Fig. 2-7B to 2-7F, 2-7B' to 2-7F', 2-7H to 2-7L, 2-7H' to 2-7L'). *Zic1* was expressed in cells in the mesenchyme adjacent to all portions of the otic epithelium except for the ventral portions of the ear and the CVG (Fig. 2-7B, 2-7B', 2-7H, 2-7H'; a blue dashed line marks the border between the otic epithelium and the surrounding mesenchyme). *Zic2* and *Zic5* expression was seen in cells in the mesenchyme that surrounded the entire otic epithelium, including the cochlea, although the expression of *Zic5* was much weaker (Fig. 2-7C, 2-7C', 2-7F, 2-7F', 2-7I, 2-7I', 2-7L, 2-7L'). Expression of *Zic3* was restricted to cells surrounding the dorsal half of the developing inner ear and was strongest in cells adjacent to the dorsolateral region of the otic epithelium (Fig. 2-7D, 2-7D', 2-7J, 2-7J'). *Zic4* expression was the most restricted of the *Zic* genes at these stages, with *Zic4*-expressing cells only detected medially in the mesenchyme between the neural tube and otic epithelium (Fig. 2-7E, 2-7E', 2-7K, 2-7K').

Identifying *Zic*-expressing cells

We examined the expression of *Axin2*, *Brn4*, *Tbx1*, and *Sox10* in sections at

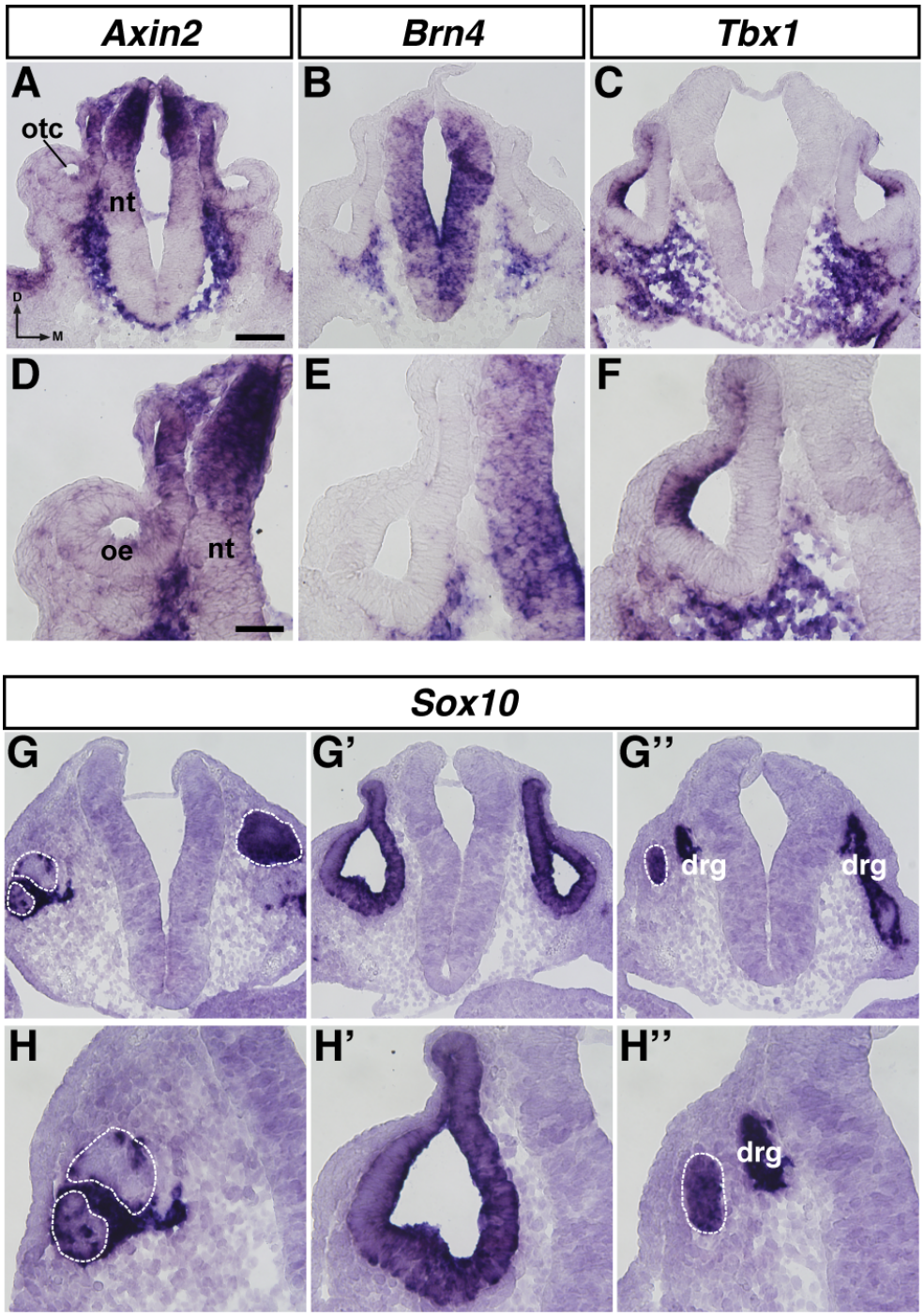

Figure 2-8. Characterization of *Zic*-Expressing Cells in the Periotic Mesenchyme of E10.5 Mouse Embryos. *In situ* hybridization on 12µm transverse sections through the otocyst of E10.5 mouse embryos using probes for *Axin2* (A, D), *Brn4* (B, E), *Tbx1* (C, F), and *Sox10* (G-G'', H-H''). Abbreviations: oe, otic epithelium; otc, otocyst; nt, neural tube; drg, dorsal root ganglion; d, dorsal; m, medial. White dashed line indicates anterior (G, H) or posterior (G'', H'') edge of otocyst. Scale bar in A, 100µm (applies to A-C, G-G''); scale bar in D, 50µm (applies to D-F, H-H'').

similar levels through the otocyst at E10.5 to attempt to characterize the *Zic*-expressing cells in the mesenchyme outside of the neuroepithelium and otic epithelium. *Axin2*, which identifies cells with active Wnt signaling (Jho, Zhang et al. 2002), was expressed in the dorsal neural tube, the dorsomedial otic epithelium, and in cells adjacent to the neural tube along its entire dorso-ventral axis (Fig. 2-8A, 2-8D). A subset of *Axin2*-expressing cells adjacent to the dorsal neural tube also expressed *Zic1-4* (*cf.* Figs. 2-6H, 2-6I, 2-6J, 2-6K and Figs. 2-8A, 2-8D). In the mesenchyme between the ventral neural tube and the otic epithelium, *Axin2* expression overlapped with the expression of *Zic1* and *Zic2* (*cf.* Figs. 2-6H, 2-6I and Figs. 2-8A, 2-8D). *Brn4*, a marker of condensing mesenchyme (Phippard, Heydemann et al. 1998; Riccomagno, Martinu et al. 2002), was expressed throughout the neural tube and in cells adjacent to the ventrolateral and ventromedial otic epithelium, but was not expressed in a band of cells immediately adjacent to the neural tube (Fig. 2-8B, 2-8E). This expression overlapped with that of *Zic1* and *Zic2* in the mesenchyme between the ventral neural tube and the otic epithelium; however, the region of *Brn4*$^{+}$ cells only partially overlapped the region of *Zic*$^{+}$ cells (*cf.* Figs. 2-6H, 2-6I and Figs. 2-8B, 2-8E). Expression of *Tbx1*, a marker of the periotic mesenchyme (Riccomagno, Martinu et al. 2002; Vitelli, Viola et al. 2003; Raft, Nowotschin et al. 2004), was also detected in the lateral wall of the otocyst, in most of the cells below the ventral otic epithelium, and between the ventral neural tube and the otic epithelium (Fig. 2-8C, 2-8F). Most of the *Brn4*-expressing cells also expressed *Tbx1*, which was expected given that *Tbx1* marks the periotic

mesenchyme, and *Brn4* is expressed in condensing cells of the periotic mesenchyme (*cf.* Figs. 2-8B, 2-8E and Figs. 2-8C, 2-8F). The mesenchymal expression of *Zic1* and *Zic2* between the ventral neural tube and the otic epithelium overlapped with *Tbx1* expression (*cf.* Figs. 2-6H, 2-6I and Figs. 2-8C, 2-8F).

Expression of *Sox10*, which identifies neural crest cells and is also expressed by cells in the otic epithelium (Watanabe, Takeda et al. 2000; Breuskin, Bodson et al. 2009; Bronner 2012), was examined at three different axial levels through the otocyst: anterior to the otocyst (Fig. 2-8G, 2-8H), through the otocyst (Fig. 2-8G2-', 8H'), and posterior to the otocyst (Fig. 2-8G'', 2-8H''). Anterior to the otocyst, *Sox10* expression was detected in the wall of the otocyst but not in the mesenchyme (Fig. 2-8G, 2-8H; white dashed lines outline the otocyst). Similar expression was observed through the otocyst (Fig. 2-8G', 2-8H'). Posterior to the otocyst, *Sox10* expression was again found in the wall of the otocyst (white dashed line) as well as in neurons of the neural crest-derived dorsal root ganglion adjacent to the neural tube (drg; Fig. 2-8G'', 2-8H'').

Taken together, these results indicate that the *Zic*$^{+}$ cells surrounding the otocyst are not neural crest cells because *Sox10* expression was not seen in the same regions in which *Zic*$^{+}$ cells were located (Fig. 2-8G, 2-8H, 2-8G', 2-8H', 2-8G'', 2-8H''). The ventral-most *Zic*$^{+}$ cells are most likely periotic mesenchyme, a subset of which is condensing cartilage (that will later form the otic capsule), because they expressed either *Tbx1* or *Tbx1* and *Brn4* (Fig. 2-8B, 2-8C, 2-8E, 2-8F). The *Zic*$^{+}$ region in the ventral mesenchyme and adjacent to the dorsal neural

tube overlapped with the *Axin2*$^{+}$ region (Fig. 2-8A, 2-8D), suggesting that WNT signaling was active in these cells.

2.4. Discussion

Distinct spatiotemporal expression of *Zic* genes during inner ear development in the chick and mouse

This study presents a comprehensive analysis of *Zic* gene expression in the developing chick and mouse inner ear. *Zic* genes from both mouse (*Zic1-5*) and chick (*Zic1-4*) were found to be expressed in similar patterns during inner ear development—in the dorsal neural tube and throughout the mesenchyme adjacent to the developing inner ear, but not in the otic epithelium. Each *Zic* gene had a unique pattern of expression at each developmental stage examined, but localized overlapping expression of multiple *Zic* genes often occurred. The timing of expression also differed, as the expression of *Zic1-5* in mouse and *Zic1-3* in chick was detected at the earliest time points analyzed in this study (E9.5 in mouse, HH stage 13 in chick), but weak expression of chick *Zic4* was not found until HH stage 18, with stronger expression seen by HH stage 24. At E9.5, expression of *Zic1 and Zic2* in mouse was seen in both the dorsal neural tube and in the mesenchyme surrounding the otic epithelium, while mesenchymal expression of *Zic3-5* in mouse and *Zic1-3* in chick was found only after the onset of expression in the neuroepithelium. The differences in spatiotemporal expression of the *Zic* genes suggests that each *Zic* gene may be playing a different role during inner ear development. *Zic2*, which is expressed in the

mesenchyme surrounding the entire otic epithelium in both mouse and chick, may be important for the overall growth and shaping of the entire developing inner ear. The other *Zic* genes, which are expressed in different regions of the periotic mesenchyme, may be responsible for growth and morphological changes associated with specific inner ear structures.

Identity and possible roles of *Zic*-positive cells in critical tissues during inner ear development

Neural Crest

Our analyses identified *Zic*-positive cells outside of the neural tube, adjacent to the otic epithelium. We considered the possibility that these cells were migrating cranial neural crest. However, several lines of evidence argue against this. Previous work in the chick demonstrated that *Zic1*-positive cells in the trunk outside of the neural tube were not labeled with HNK-1, a marker of migratory neural crest cells (Sun Rhodes and Merzdorf 2006). Additionally, the timing, location, and neural crest marker expression of these cells does not correlate with that of migrating cranial neural crest cells. In the mouse, cranial neural crest cells form and begin migrating at the 5 somite stage (Chan and Tam 1988) and finish migrating by the 14 somite stage (Serbedzija, Bronner-Fraser et al. 1992), while in the chick, neural crest cells migrate from HH stage 9+ to HH stage 11 (Tosney 1982). The Zic^{+} cells we detected in the mesenchyme were seen in much older embryos—22-24 somite stage (E9.5) and older in the mouse, and HH

stage 18 and older in the chick. Second, DiI labeling studies in chick embryos and lineage tracing studies in mouse embryos indicate that neural crest cells from rhombomere 5 migrate rostrally and caudally around the otocyst and arrive in the second and third branchial arches, while neural crest cells from rhombomere 6 migrate caudally around the otocyst before arriving in the third branchial arch (Sechrist, Serbedzija et al. 1993; Trainor, Sobieszczuk et al. 2002). The sections in which *Zic*$^{+}$ cells were detected in the mesenchyme were taken midway through the otocyst in a region where neural crest cells do not migrate. Finally, we used *Sox10* expression as a marker for migrating neural crest cells in the mouse (Bronner 2012). *Sox10* expression was not detected outside of the otic epithelium in sections through the medial portion of the otocyst at E10.5, but was found in sections at the most anterior or posterior levels of the otocyst. *Zic1-4*$^{+}$ cells at E10.5 were detected outside of the neural tube in sections through the medial portions of the otocyst, suggesting that these *Zic*-expressing cells were not of neural crest origin.

Periotic Mesenchyme

We examined the expression of *Brn4* and *Tbx1*, markers of condensing mesenchyme and periotic mesenchyme, in the regions where we found *Zic*-expressing cells. The region of *Tbx1* expression overlapped with the regions of *Zic1* and *Zic2* expression, but the region of *Brn4* expression only overlapped slightly with the regions of *Zic1* and *Zic2* expression. This suggests that the majority of *Zic1*$^{+}$ and *Zic2*$^{+}$ cells in the ventral mesenchyme are *Tbx1*$^{+}$ periotic

mesenchyme cells, and a few of these cells are *Brn4*$^{+}$ cells of the condensing mesenchyme. Expression of *Tbx1* and *Brn4* is regulated by SHH signaling (Riccomagno, Martinu et al. 2002), and *Zic* genes regulate SHH signaling *in vitro* (Koyabu, Nakata et al. 2001; Mizugishi, Aruga et al. 2001; Pan, Gustafsson et al. 2011), so the expression of *Zic* genes in the same regions where *Tbx1* and *Brn4* are expressed could mean that the *Zic* genes are involved in the SHH-dependent expression of *Tbx1* and *Brn4*. Alternatively, the *Tbx1* and *Brn4* expression could be independent of *Zic* expression, suggesting a different role for the *Zic* genes. *Zic* genes, like *Tbx1* and *Brn4*, could be required for proper epithelial-mesenchymal signaling. Loss of either *Brn4* (*Brn4*$^{-/-}$) or *Brn4* and a single allele of *Tbx1* (*Brn4*$^{-/-}$;*Tbx1*$^{+/-}$) in the periotic mesenchyme in mice results in improper coiling of the cochlea (Braunstein, Crenshaw et al. 2008). Loss of one or multiple *Zic* genes in the periotic mesenchyme could result in similar defects in inner ear structures, with the specific structures affected depending on which *Zic* gene is lost.

We also examined *Axin2* expression in the mesenchyme. The dorsal-most expression of *Axin2* overlapped with the expression of *Zic1-4*, while the ventral expression overlapped with the expression of *Zic1* and *Zic2*. *Axin2* expression induced by WNT signaling acts as part of a negative feedback loop to limit the extent and duration of WNT signaling (Jho, Zhang et al. 2002). WNT signaling from the dorsal hindbrain and SHH signaling from the notochord and floor plate pattern the otocyst along its dorsal-ventral axis and are critical for the development of the dorsal (WNT) and ventral (SHH) structures of the inner ear

(Riccomagno, Martinu et al. 2002; Riccomagno, Takada et al. 2005). *In vitro,* ZIC2 binding to TCF4 inhibits WNT signaling (Pourebrahim, Houtmeyers et al. 2011), so the combination of *Axin2* expression and *Zic* expression may selectively modulate WNT signals from the dorsal hindbrain to the otocyst as well as restricting ventral WNT signals closer to the source of SHH. Additional experiments are needed to determine this, as well as co-labeling experiments to determine whether the Zic^{+} mesenchymal cells are $Axin2^{+}/Tbx1^{+}/Brn4^{+}/Sox10^{-}$ as would be expected.

Neural Tube

In both chick and mouse, all *Zic* genes (chick *Zic1-4*, mouse *Zic1-5*) were expressed in the dorsal neural tube. The inner ear lies adjacent to the neural tube, and alterations in specification and patterning of the neural tube are known to affect inner ear development. Signaling from the hindbrain, especially rhombomeres 5 and 6, is critical for proper patterning and development of the inner ear, as well as development of the cochleovestibular ganglion that innervates the ear (Bok, Bronner-Fraser et al. 2005; Kil, Streit et al. 2005; Bok, Brunet et al. 2007; Choo 2007; Vazquez-Echeverria, Dominguez-Frutos et al. 2008; Liang, Bok et al. 2010). Neural tube closure defects, including exencephaly, in or near the hindbrain, are seen in *Zic* mutant mice examined to date, including $Zic2^{kd/kd}$ (Nagai, Aruga et al. 2000), $Zic3^{Bn}$ (Klootwijk, Franke et al. 2000) and $Zic5^{-/-}$ (Inoue, Hatayama et al. 2004) mutant mice. In $Zic2^{Ku/Ku}$ mutants, rhombomeres 3 and 5 are smaller than those in wild type embryos, and

ectopic *follistatin* expression is detected in these rhombomeres (Elms, Siggers et al. 2003). In addition to effects on hindbrain development, mutations in *Zic* genes affect signaling from the hindbrain to the inner ear. Expression of *Wnt3a*, a signaling molecule from the hindbrain important for inner ear development (Riccomagno, Takada et al. 2005), is delayed in the dorsal hindbrain of both *Zic2*$^{kd/kd}$ (Nagai, Aruga et al. 2000) and *Zic5*$^{-/-}$ (Inoue, Hatayama et al. 2004) mutant mice. *Zic* genes expressed in the neural tube could effect inner ear development in multiple ways, both directly and indirectly. ZIC proteins could directly interact with WNT or BMP pathway components in the neural tube to modulate WNT or BMP signaling to the developing inner ear, or ZIC proteins could promote/inhibit the expression of other factors in the dorsal neural tube. Indirectly, loss of specific Zic genes in the neural tube leads to neural tube defects (such as exencephaly), which would alter the position of the neural tube relative to the inner ear. This change in position of the neural tube relative to the developing inner ear would alter the position of specific regions of the otic epithelium relative to sources of BMP, WNT, and SHH signaling, potentially leading to malformations of the inner ear.

Investigating the function of *Zic* genes during inner ear development

To date, the involvement of *Zic* genes in inner ear development has only been examined at the level of gene expression (this study; Warner, Hutson et al. 2003). Further functional studies are needed to investigate the role of the *Zic* genes during inner ear development. Mice with mutations in each of the *Zic*

genes have been generated (Ali, Bellchambers et al. 2012), but no ear phenotypes have been reported to date. One reason for this could be that multiple severe defects in the postnatal animals mask any ear phenotypes. Both *Zic1* and *Zic5* homozygous mutants display abnormal gait and posture characteristic of defects in the vestibular region of the inner ear, but these abnormalities were attributed to cerebellar defects (*Zic1*$^{-/-}$) or hydrocephalus (*Zic5*$^{-/-}$) (Aruga, Minowa et al. 1998; Inoue, Hatayama et al. 2004). However, the majority of *Zic5* mutants did not have any noticeable changes in brain morphology, so the cause of the abnormal gait and posture was never fully investigated (Inoue, Hatayama et al. 2004). Another reason an inner ear phenotype has not been characterized is that significant numbers of mutants die, either during embryonic stages (all *Zic2*$^{Ku/Ku}$, ~24% of *Zic3*^{Bn}) or shortly after birth (50% of *Zic1*$^{-/-}$, all *Zic2*$^{kd/kd}$, some *Zic5*$^{-/-}$) (Aruga, Minowa et al. 1998; Klootwijk, Franke et al. 2000; Nagai, Aruga et al. 2000; Elms, Siggers et al. 2003; Inoue, Hatayama et al. 2004), making it impossible to detect signs of inner ear defects that affect the mature function of this sensory organ, such as changes in gait or posture, abnormal behaviors such as circling, and changes in the acoustic startle response or auditory brainstem responses (ABR) (Saul, Brzezinski et al. 2008). Studies using these mice, including recording of ABRs in any animals, including heterozygotes, that live to postnatal stages, as we have done for other mouse mutations (Bank, Bianchi et al. 2012) could provide insights into how individual *Zic* genes function during inner ear development. Further, the generation of compound *Zic* mutants would be useful to address questions of redundancy

among the *Zic* genes during inner ear development, as we have shown that the *Zic* genes are expressed in overlapping regions of the periotic mesenchyme in both chick and mouse.

Attempts to reconcile the disparate results of earlier *Zic* gene expression studies

Because the results found by McMahon and Merzdorf (McMahon and Merzdorf 2010) were found to be distinctly different from those of our earlier report (Warner, Hutson et al. 2003), particularly for the expression of *Zic1*, we repeated and expanded the expression study of the *Zic* genes in the developing chick inner ear. A fourth *Zic* gene, *Zic4*, has since been identified in the chicken (McMahon and Merzdorf 2010) and its expression pattern was also examined. In addition, we wanted to compare the expression of the *Zic* genes in the otic region of the chicken to the expression pattern of the *Zic* genes in the otic region of the mouse, which had not previously been reported. To our surprise, the expression pattern of *Zic1* in the developing chick inner ear we report here is not consistent with our earlier study; however, the expression patterns of *Zic2* and *Zic3* reported here are consistent with our earlier study (Warner, Hutson et al. 2003). Our findings for the expression patterns of *Zic1-4* in the neural tube of the developing chick in the present study are consistent with an earlier study examining the expression of *Zic1-4* in the developing chick embryo up to HH stage 18 (McMahon and Merzdorf 2010). However, we found expression of both *Zic1* and *Zic2* in the periotic mesenchyme at HH stage 18, whereas McMahon and

Merzdorf only saw *Zic2* expression in the periotic mesenchyme (McMahon and Merzdorf 2010). An explanation for this is that at HH stage 18, we detected periotic mesenchyme expression in sections taken through the ear, which allowed us to examine expression patterns in locations that would not have been discernable in the whole mounts used in the other study (McMahon and Merzdorf 2010). This leaves us to question the differences in *Zic1* expression in the developing chick inner ear that were seen in this study as contrasted with our previous study (Warner, Hutson et al. 2003). All probes (this study and the previous study; Warner, Hutson et al. 2003) were sequenced to confirm their identity. In this study, the probes were designed to target sequences outside of the zinc finger region where there is low homology between the *Zic* genes (Fig. 2-3). Both the chick *Zic2* and *Zic3* probes used in this study target similar regions as the *Zic2* and *Zic3* probes from our previous study (Warner, Hutson et al. 2003). The *Zic2* probes each target a different part of the 3' untranslated region (UTR) of the mRNA. Similarly, the *Zic3* probes target an overlapping region of the 3' UTR, with the probe used in this study also extending both into a portion of the 3' coding region of the mRNA and further into the 3' UTR. The *Zic1* probe used in our earlier study targeted the zinc finger region of *Zic1*, and this likely underscores the differences with the earlier study. The probe used in this study targets the 3'UTR of *Zic1* and excludes this zinc finger region.

We believe this more detailed and thorough study now resolves the differences between the two earlier studies, confirming the Merzdorf lab's findings of the lack of *Zic1* expression in the developing chick embryonic inner

ear, confirming the expression patterns we found in the developing chick inner ear for *Zic2* and *Zic3* and extending the study of the chick *Zic* gene expression in the region of the developing otic region and the neural tube to characterize the expression pattern of *Zic4*. We have further extended the study of otic/periotic/neural tube expression of the *Zic* genes to the mouse, as a prelude to examining such expression in *Zic* mutant embryos and animals.

2.5. Experimental Procedures

Mouse Embryos

Wild type Balb/c mice were used to set up timed matings. Noon on the day on which a vaginal plug was detected was designated as E0.5. Pregnant females were sacrificed by cervical dislocation. All experiments using mice were approved by the Animal Use and Care committee of the University of Michigan and conform to all guidelines of the Unit for Laboratory Animal Medicine and those of the National Institutes of Health. The uterine horns containing the embryos were dissected out and placed in PBS with 10% FBS. Embryos were then dissected out of the surrounding maternal tissues and Reichert's membrane was removed. Embryos were fixed in 4% paraformaldehyde (PFA) overnight, washed in 1X PBS (3 x 5 minutes), and then transferred to 30% sucrose in 1X PBS and rocked at 4°C overnight.

Chick Embryos

Fertilized White Leghorn chicken eggs were obtained from the Michigan State University Poultry Farm (East Lansing, MI), and placed in a humidified incubator at 37°C. Eggs were windowed and the embryos were dissected and placed into PBS with 10% FBS. The vitelline membrane was removed and embryos were dissected out of the amnion. Embryos were fixed in 4% PFA overnight, washed in 1X PBS (3 x 5 minutes), and then transferred to 30% sucrose in 1X PBS and rocked at 4°C overnight.

Embedding and Cryosectioning

Embryos were transferred through three progressive changes of OCT (TissueTek) to remove excess sucrose. The embryos were then transferred to embedding molds, covered with OCT, and oriented such that the anterior portion of the ear pointed down. The molds were then frozen on dry ice and stored at -80^{o}C until sectioning. 12µm or 25µm transverse sections through the ear were cut using a Microm HM500M cryostat and collected on SuperFrost Plus slides (Fisher). Sections were air-dried on the slides at room temperature for at least 30 minutes, and then stored at -80^{o}C.

***In situ* Hybridization**

In situ hybridization using digoxigenin-labeled antisense probes was performed on sections using a protocol adapted from Wilkinson and Nieto (Wilkinson and Nieto 1993). The pre-hybridization, hybridization, and post-hybridization steps

were performed essentially as described, except MBST (100mM Maleic Acid, 150mM NaCl, 0.1% Tween20) was used for the post-hybridization washes and the blocking solution was MBST containing 10% heat-inactivated sheep serum and 2% Blocking Reagent (Roche). For the color reaction, BM Purple (Roche) was used instead of NBT/BCIP. Following the color reaction, slides were washed three times in PBST, pH 4.5 (PBS with 0.1% Tween20), fixed (4% PFA/0.2% gluteraldehyde), washed three times in PBS, dehydrated in 70% ethanol, and dried on a slide warmer set at 60^{o}C. Sections were then mounted under a coverslip with Glycergel Mounting Media (Dako). A minimum of 4 embryos was analyzed for each probe. Antisense probes were generated by digesting plasmids containing the cDNA sequences of either the mouse or chick genes and then transcribing with the appropriate RNA polymerase. Probes for chick *Zic3* and chick *Zic4* were prepared by PCR as previously described (McMahon and Merzdorf 2010). Both the mouse and chick *Zic* probes were designed to target sequences outside of the zinc finger region where there is lower homology between the *Zic* genes (Fig. 3). Images were acquired with an Olympus BX51 microscope equipped with an Olympus camera.

Phylogenetic Tree and Sequence Analysis

The complete amino acid sequence of the *Zic* genes from human, mouse, chick, zebrafish, and frog were aligned with the amino acid sequence of the ancestral gene *odd-paired* (*opa*) from *Drosophila* using Clustal Omega (http://www.ebi.ac.uk/Tools/msa/clustalo). The alignment was then converted into

a phylogenetic tree using Tree Vector (http://supfam.cs.bris.ac.uk/TreeVector). Pairwise comparisons of the amino acid sequences of human, mouse, and chick *Zic* genes was performed using EMBOSS Stretcher (http://www.ebi.ac.uk/Tools/psa/emboss_stretcher).

Chapter 3

The Role of *Zic* Genes in Inner Ear Development in the Mouse

3.1. Abstract

Background: In the mouse, *Zic* genes (*Zic1-5*) are expressed in the dorsal hindbrain and to varying degrees in the periotic mesenchyme adjacent to the epithelium of the developing inner ear. *Zic* genes are known to be involved in developmental signaling pathways in many systems, though the exact role of *Zic* in such pathways has not yet been elucidated. These same signaling pathways are known to be key to inner ear development. This report examines the role of *Zic1*, *Zic2*, and *Zic4* during inner ear development in the mouse. Results: *Zic1*/*Zic4* double mutants do not exhibit any apparent defects in inner ear morphology during development, while inner ears from both $Zic2^{kd/kd}$ and $Zic2^{Ku/Ku}$ mutants have severe but variable morphological defects. Analysis of otocyst patterning in the $Zic2^{Ku/Ku}$ mutants by *in situ* hybridization using probes to detect *Dlx5*, *Gbx2, Pax2,* and *Lfng* showed no changes in the expression of these genes in the $Zic2^{Ku/Ku}$ mutants. Conclusions: *Zic1* and *Zic4* are dispensable for normal morphological development of the inner ear. In contrast, partial ($Zic2^{kd/kd}$) or complete ($Zic2^{Ku/Ku}$) loss of *Zic2* results in severe inner ear defects. Complete loss of *Zic2* ($Zic2^{Ku/Ku}$) did not affect otocyst patterning.

3.2. Introduction

The *Zic* genes, particularly *Zic1* and *Zic2*, are involved in many different phases of development, especially as part of regulatory networks that influence neural development (reviewed in Aruga 2004; Merzdorf 2007; Ali, Bellchambers et al. 2012; Houtmeyers, Souopgui et al. 2013). More than 15 years ago, a study showed that *Zic2* expression was upregulated in the sensory epithelium of the chick following noise trauma, indicating that *Zic2* may be involved in post-injury repair and possibly in regeneration of the auditory epithelium (Gong, Hegeman et al. 1996). Because regeneration in many cases mirrors developmental events, it is possible that genes involved in post-injury repair or possibly in regeneration of a tissue are also involved during its normal development, making the *Zic* genes—and *Zic2* in particular—candidates for involvement in inner ear development. Although this early study implicates *Zic2* in sensory epithelium post-injury healing and possibly regeneration, to date very little work has been done to investigate the link between *Zic* genes and inner ear development. Previously published work showed that *Zic1*, and not *Zic2*, was expressed in the otic epithelium during inner ear development in the chick, indicating that normal ear development and regeneration following damage to the inner ear could involve different *Zic* genes (Warner, Hutson et al. 2003). However, another study examining the expression patterns of the *Zic* genes in the entire developing chick embryo found a different expression pattern surrounding the developing inner ear (McMahon and Merzdorf 2010). To reconcile these differences and to expand the expression pattern of the *Zic* genes during inner ear development to another organism, we examined

the expression patterns of *Zic1-5* (mouse) and *Zic1-4* (chick) in the region of the developing inner ear (Chervenak, Hakim et al. 2013). We showed that although the *Zic* genes are expressed in the dorsal hindbrain and periotic mesenchyme adjacent to the developing inner ear, none of them is expressed in the developing otic epithelium, in either the mouse or the chick, and that the expression patterns vary among the different *Zic* genes for mouse and chick (Chervenak, Hakim et al. 2013).

We found that *Zic2* was the most widely expressed of the *Zic* genes in both mouse and chick, with expression detected in the mesenchyme completely surrounding the developing inner ear in both species, as well as in the dorsal neural tube adjacent to the developing inner ear (Chervenak, Hakim et al. 2013). Each *Zic* gene has a unique spatiotemporal expression pattern during inner ear development, but the expression and timing of expression of individual *Zic* genes partially overlap with one another (Chervenak, Hakim et al. 2013). Based on their spatiotemporal expression patterns, we hypothesized that *Zic1* and *Zic3-5* may have roles in the development of specific regions of the inner ear, while *Zic2*, which we have found to be expressed in the periotic mesenchyme surrounding the entire developing inner ear in both mammals and birds (Chervenak, Hakim et al. 2013) may have a more global role to play in inner ear development and morphological patterning. *Zic* genes could regulate BMP or WNT signaling pathways in, or emanating from, the dorsal hindbrain, participate in mesenchymal-epithelial signaling, or have a novel—and as yet unidentified—function during the development of the inner ear.

The function of the *Zic* genes during inner ear development therefore remains to be investigated. In this study we have focused on the possible function(s) of *Zic2* during inner ear development through an initial analysis of mice in which the *Zic2* gene has been mutated. We analyzed two mouse models in which the *Zic2* gene is modified: the first is $Zic2^{kd}$, a hypomorphic allele of *Zic2* (Nagai, Aruga et al. 2000), and the second is $Zic2^{Kumba}$, a complete loss-of-function allele of *Zic2* that results in embryonic lethality shortly after E12.5 in homozygotes (Elms, Siggers et al. 2003). We also analyzed inner ears from *Zic1*/*Zic4* compound mutants (Grinberg, Northrup et al. 2004; Blank, Grinberg et al. 2011), but did not find any defects in inner ear morphology.

3.3. Results

Morphological Analysis of Inner Ears from *Zic* Mutant Mice

Zic1/*Zic4*

Ears from $Zic1^{+/-}$;$Zic4^{+/-}$ and $Zic1^{-/-}$;$Zic4^{-/-}$ mouse embryos at E11.5 (Figure 3-1A, B) and E15.5 (Figure 3-1C, D) were paint-filled to examine changes in inner ear morphology. The combined loss of *Zic1* and *Zic4* had no noticeable effect on the structures of the inner ear at the times examined (E11.5 and E15.5; *cf*. Figure 3-1B and Figure 3-1A; *cf*. Figure 3-1D and Figure 3-1C).

$Zic2^{kd}$

Paint-filled inner ears from $Zic2^{+/+}$, $Zic2^{kd/+}$, and $Zic2^{kd/kd}$ embryos were compared

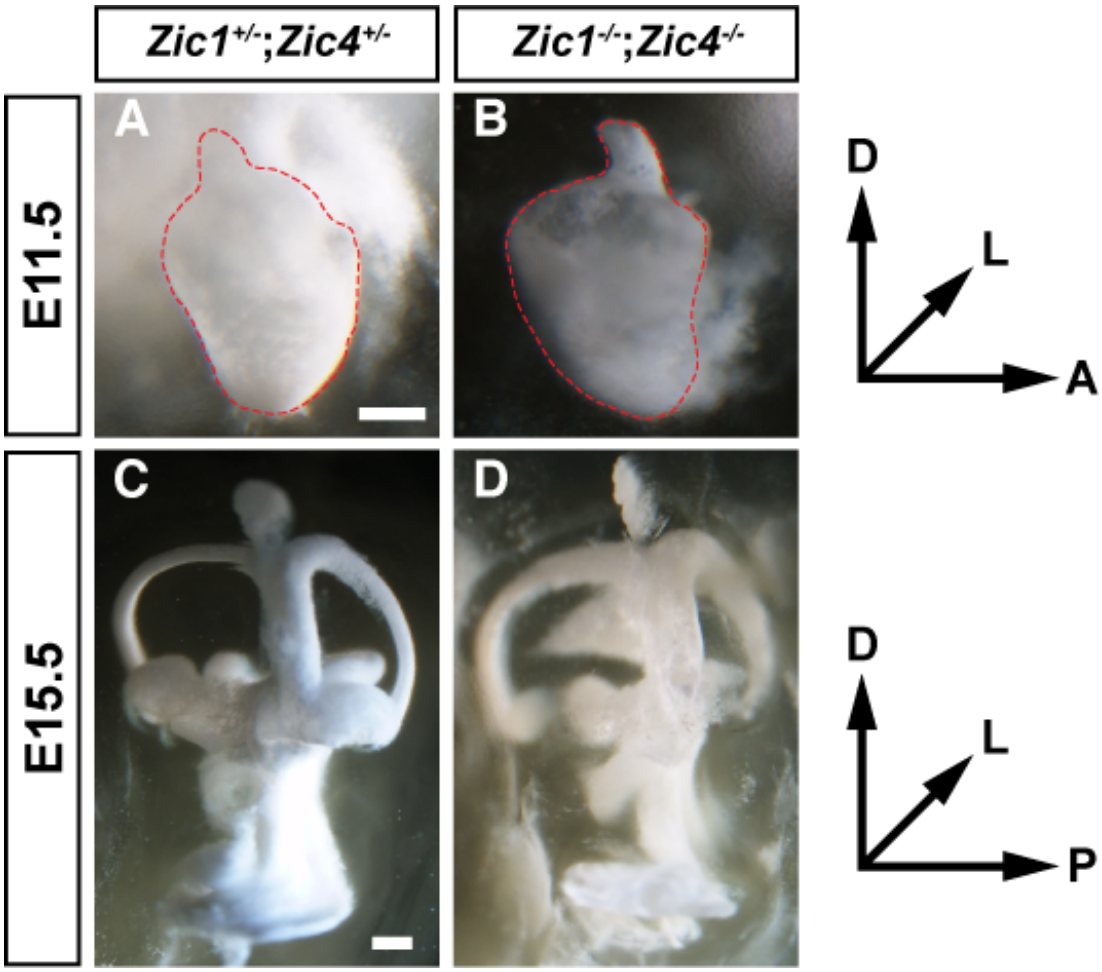

Figure 3-1. Morphology of Inner Ears From *Zic1*/*Zic4* Mice. Ears from *Zic1*$^{+/-}$;*Zic4*$^{+/-}$ (A, C) and *Zic1*$^{-/-}$;*Zic4*$^{-/-}$ (B, D) mice were paint-filled at E11.5 (A,B) and E15.5 (C, D) to look for changes in inner ear morphology. Abbreviations: D, dorsal; L, lateral; A, anterior; P, posterior. Scale bar in A, 100μm (applies to A, B); scale bar in C, 200μm (applies to C, D). **[E11.5: n=4 ears for both genotypes; E15.5: n=n5 ears for both genotypes]**

---

at E11.5, E13.5, E16.5, and E18.5 (Figure 3-2). At E11.5 when the endolymphatic duct normally begins to emerge from the dorsal surface of the otocyst and the cochlear duct emerges ventrally, no morphological differences are detected in the inner ears of *Zic2*$^{kd/kd}$ embryos (*cf*. Figure 3-2A and Figure 3-2B). The inner ear undergoes further morphological changes, including the

formation of the semicircular canals and the coiling of the cochlea, and by E13.5, the inner ear has assumed its distinctive shape. Wild type (Figure 3-2C) and heterozygous (Figure 3-2D) embryos have inner ears that contain all structures, including the three semicircular canals (anterior, lateral, and posterior), the endolymphatic sac, cochlea, saccule, and the utricle, which cannot be seen in this view of the ears. In contrast, the inner ears from *Zic2*$^{kd/kd}$ embryos (Figure 3-2E) lack the endolymphatic duct/sac, have missing or incomplete semicircular canals, and have a cochlea that initially grows dorsally rather than anteriorly (*cf*. Figure 3-2E and Figure 3-2C, Figure 3-2D). Further refinements to the inner ear structures occur by E16.5, including outgrowth and coiling of the cochlea, and these changes are evident in the wild type inner ear (Figure 3-2F). In comparison, the inner ear from the *Zic2*$^{kd/kd}$ embryo has an indeterminate shape, with a failure of most of the structures to develop, though a partial semicircular canal has formed, as has a rudiment of the cochlea (Figure 3-2G). Comparisons of the inner ears from the *Zic2*$^{kd/kd}$ embryos at E13.5 (Figure 3-2E) and E16.5 (Figure 3-2G) show variability in the severity of the inner ear phenotype. At E18.5, the cochlea has coiled further in the wild type inner ear (Figure 3-2H). Inner ears from *Zic2*$^{kd/kd}$ embryos again show a variability in the severity of the phenotype, with some ears only missing one semicircular canal and having a slightly deformed cochlea (Figure 3-2I), while others are missing multiple semicircular canals and the saccule and have a more severely affected cochlea (Figure 3-2J).

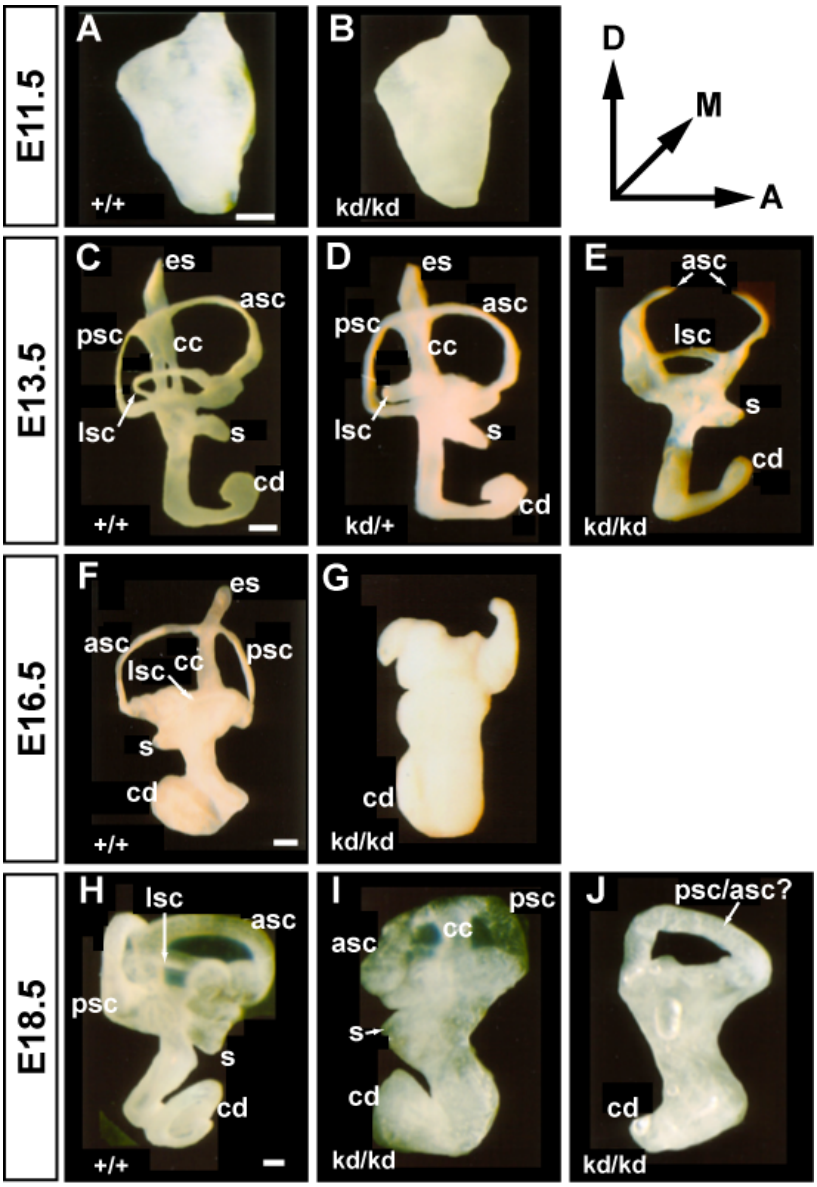

Figure 3-2. Reduced Levels of *Zic2* Result in Severe Inner Ear Morphological Defects. Ears from *Zic2*$^{+/+}$ (A, C, F, H), *Zic2*$^{kd/+}$ (D), and *Zic2*$^{kd/kd}$ (B, E, G, I, J) embryos were paint-filled at E11.5 (A,B), E13.5 (C-E), E16.5 (F, G) and E18.5 (H-J) to look for changes in inner ear morphology. At E18.5, the ducts appear thicker due to a perilymphatic rather than endolymphatic-only fill (Kiernan 2006). Abbreviations: D, dorsal; M, medial; A, anterior; es, endolymphatic sac; cc, common crus; asc, anterior semicircular canal; psc, posterior semicircular canal; lsc, lateral semicircular canal; s, saccule; cd, cochlear duct. Scale bar in A, 100μm (applies to A, B); scale bar in C, 200μm (applies to C-E); scale bar in F, 200μm (applies to F, G); scale bar in H, 200μm (applies to H-J). **[E11.5: n=4 ears for both genotypes; E13.5: n=4 ears (*Zic2*$^{+/+}$, *Zic2*$^{kd/+}$), 6 ears (*Zic2*$^{kd/kd}$); E16.5: n=6 ears (*Zic2*$^{+/+}$, *Zic2*$^{kd/kd}$), 4 ears (*Zic2*$^{kd/+}$); E18.5: n=4 ears (*Zic2*$^{+/+}$), 12 ears (*Zic2*$^{kd/+}$) 6 ears (*Zic2*$^{kd/kd}$]. *Data generated by Lisa Gerlach-Bank***

Zic2^{Ku}

Inner ears from *Zic2*$^{+/+}$, *Zic2*$^{Ku/+}$, and *Zic2*$^{Ku/Ku}$ embryos were also paint-filled at E11.5 and E12.5 to look for changes in inner ear morphology (Figure 3-3). At E11.5, the gross morphology of inner ears from heterozygotes (Figure 3-3B) looked normal compared to those from wild type embryos (Figure 3-3A). Inner ears from *Zic2*$^{Ku/Ku}$ mutants were noticeably smaller and had truncated endolymphatic ducts and cochleae compared to either wild type or heterozygous littermates (*cf*. Figure 3-3C and Figures 3-3A, 3-3B). To quantify the size differences observed in the *Zic2*$^{Ku/Ku}$ inner ears, we measured and compared the length and width of the inner ears from *Zic2*$^{+/+}$, *Zic2*$^{Ku/+}$, and *Zic2*$^{Ku/Ku}$ embryos (Figure 3-3F, G, H). *Zic2*$^{Ku/Ku}$ inner ears were significantly smaller along both axes when compared to *Zic2*$^{+/+}$ and *Zic2*$^{Ku/+}$ littermates, and *Zic2*$^{Ku/+}$ ears were significantly shorter along their dorsal-ventral axis when compared to wild type ears (Figure 3-3G, H).

At E12.5, inner ears from *Zic2*$^{Ku/Ku}$ mutants were even smaller compared to those from heterozygotes, but the mutant ears had roughly the same morphological features as those seen in the heterozygotes (*cf*. Figure 3-3E and Figure 3-3D). In addition, inner ears from the *Zic2*$^{Ku/Ku}$ mutants were rotated ~90°, such that the endolymphatic duct pointed laterally instead of dorsally. We could not quantify the differences in size at E12.5 between the inner ears from *Zic2*$^{Ku/Ku}$ mutants and wild type and heterozygous littermates as we did not have sufficient sample sizes to perform the analysis, and we could not analyze inner ear morphology at later time-points, as *Zic2*$^{Ku/Ku}$ mutants die shortly after E12.5.

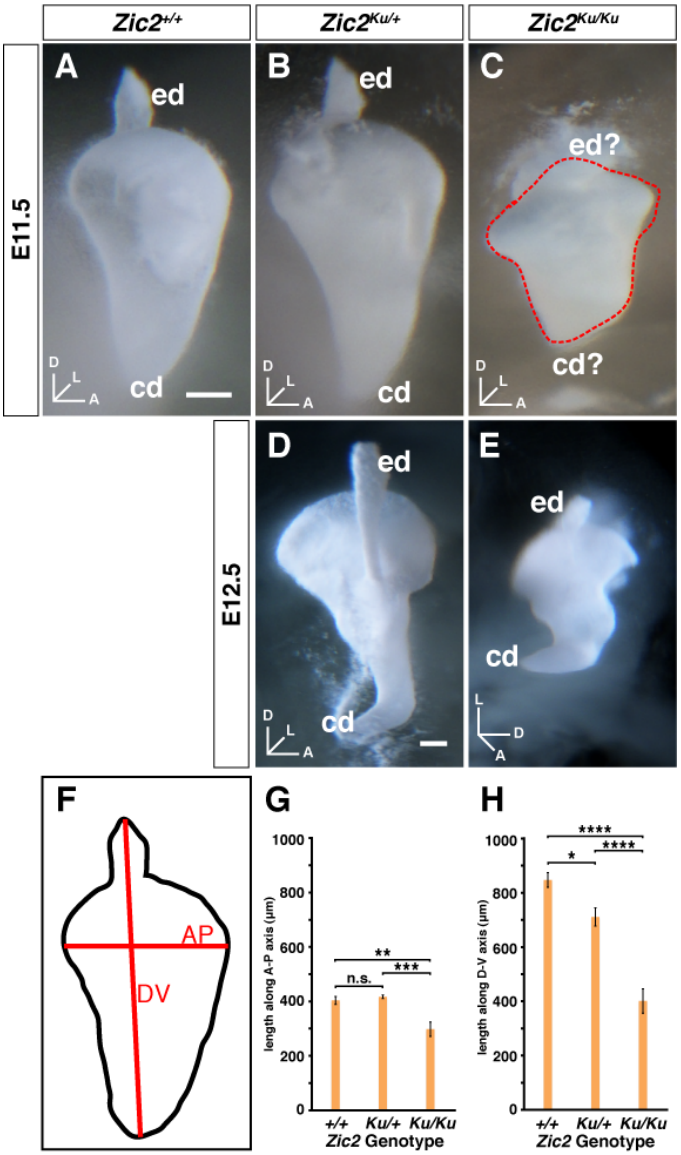

Figure 3-3. Analysis of Inner Ear Morphology From *Zic2*$^{Ku/Ku}$ Mice. Inner ears from *Zic2*$^{+/+}$ (A), *Zic2*$^{Ku/+}$ (B, D), and *Zic2*$^{Ku/Ku}$ (C, E) mouse embryos at E11.5 (A-C) and E12.5 (D, E) were paint-filled to assess changes in gross morphology. Measurements were taken along the anterior-posterior and dorsal-ventral axes of inner ears at E11.5 as shown in (F) and compared among the three genotypes. Comparison of ear dimensions along the anterior-posterior (G) and dorsal-ventral (H) axes. p-values are designated in the figure as follows: *, p <0.05; **, p<0.05; ***, p<0.005; ****, p<0.0001; n.s., not significant. Error bars in G and H represent the SEM. Abbreviations: D, dorsal; L, lateral; A, anterior; AP, anterior-posterior; DV, dorsal-ventral; ed, endolymphatic duct; cd, cochlear duct. Scale bar in A, 100μm (applies to A-C); scale bar in D, 100μm (applies to D-E). **[E11.5: n=16 ears (*Zic2*$^{+/+}$), 19 ears (*Zic2*$^{Ku/+}$), and 4 ears (*Zic2*$^{Ku/Ku}$); E12.5: n=2 ears (*Zic2*$^{Ku/+}$, *Zic2*$^{Ku/Ku}$)]**

Rationale For Analyzing the Inner Ear Phenotypes in the *Zic2*^{Kumba} Mice

The *Zic1*/*Zic4* double mutants did not display any obvious gross defects in inner ear morphology, so we focused our analysis on the *Zic2* mutants, which did show dramatic morphological phenotypes in the inner ears. We wanted to investigate the molecular causes of the inner ear defects in both of the *Zic2* mutants, but, with the exception of the fixed specimens we received from the Aruga lab and subsequently paint-filled, the *Zic2*^{kd} mice were unavailable to us. Instead, we focused our analysis on the *Zic2 Kumba* mice. The *Kumba* mutant allele of *Zic2* behaves as a complete loss-of-function allele, and embryos homozygous for this mutation are severely affected, with noticeable effects on embryo growth and neural tube closure. The next sections discuss the effect of *Zic2* loss on the overall morphology of the embryo, as well as investigate its effects on inner ear development at the molecular level.

Gross Morphology of *Zic2*$^{Ku/Ku}$ Embryos

The nervous system of the homozygous *Zic2*^{Kumba} embryos is profoundly affected in this mouse model. By E9.5, the embryos exhibit an open neural tube, exencephaly and holoprosencephaly, and a “kinked” neural tube throughout the trunk of these embryos. Initial descriptions of the *Zic2*^{Kumba} phenotype characterized post-natal and adult heterozygotes as having a mild but variable phenotype that included curled or “kinked” tails, ventral spots, and spina bifida in a small proportion of the mice. These morphological effects (kinked tail, cyclopia, hematomas) in the *Zic2*$^{Ku/Ku}$ mutants were detailed previously (Elms, Siggers et

al. 2003). We observed the same defects in the *Zic2*$^{Ku/Ku}$ mutant embryos at E9.5 (Figure 3-4), E11.5 (Figure 3-5), and E12.5 (Figure 3-6). As observed in the initial study, we found variations in the extent, severity, and number of abnormalities present in individual embryos (Elms, Siggers et al. 2003).

We extended our analysis to include an examination of the gross morphology of the developing inner ears to identify any changes in their external appearance or location and to compare them with our earlier findings (Chervenak, Hakim et al. 2013).

At E9.5, the *Zic2*$^{Ku/Ku}$ mutants are easily distinguished from their wild type and heterozygous littermates due to large regions where the neural tube fails to close (arrowheads in Figure 3-4C). The overall size of the *Zic2*$^{Ku/Ku}$ mutants, however, is not noticeably different from that of their *Zic2*$^{+/+}$ or *Zic2*$^{Ku/+}$ littermates (*cf*. Figure 3-4C and Figure 3-4A, 3-4B). Similarly, the overall size and shape of the otocyst in *Zic2*$^{Ku/Ku}$ mutants are indistinguishable from that of wild type or heterozygous littermates (*cf*. Figure 3-4C' and Figure 3-4A', 3-4B'). In *Kumba* mutants in which the neural tube fails to close properly in the region of the hindbrain, the distance between the otocysts was greater than in *Zic2*$^{+/+}$ and *Zic2*$^{Ku/+}$ littermates (*cf*. Figure 3-4C'' and Figure 3-4A'', 3-4B''). Outside of the ear, *Zic2*$^{Ku/Ku}$ mutants displayed exencephaly in the midbrain (Figure 3-4D), malformation of the forebrain, including hematomas (yellow arrows in Figure 3-4D'), and a kinked neural tube in the trunk region of the embryo (Figure 3-4D'').

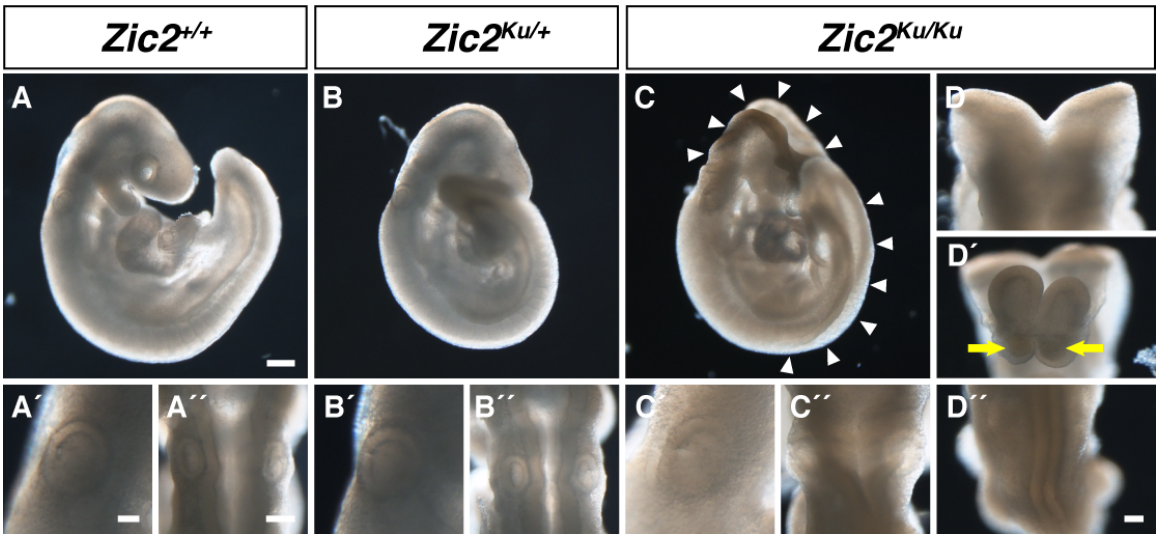

Figure 3-4. Gross Morphology of *Zic2*^{Kumba} Embryos at E9.5. *Zic2*$^{+/+}$ (A-A'') and *Zic2*$^{Ku/+}$ (B-B'') embryos show no gross morphological defects at E9.5. *Zic2*$^{Ku/Ku}$ embryos (C-C'', D-D'') have severe defects in the forebrain, midbrain, hindbrain and caudal regions of the neural tube (arrowheads in C). Higher magnification images show exencephaly in the midbrain (D), malformation of the forebrain, including hematomas (D'; yellow arrows indicate hematomas), and a kinked neural tube in the trunk region of the embryo (D''). The otocysts appear to be normal in size and shape in *Zic2*$^{+/+}$ (A'), *Zic2*$^{Ku/+}$ (B'), and *Zic2*$^{Ku/Ku}$ (C') embryos. However, the paired otocysts from *Zic2*$^{+/+}$ (A'') and *Zic2*$^{Ku/+}$ (B'') embryos are located near the midline, while otocysts from *Zic2*$^{Ku/Ku}$ embryos (C'') are located farther away from the midline due to the failure of the neural tube to close. Scale bar in A equals 200μm and applies to panels A-C; scale bar in A', 50μm (applies to panels A', B', C'); scale bar in A'', 100μm (applies to panels A'', B'', C''); scale bar in D'', 100μm (applies to panels D-D''). **[n=5 for each genotype]**

As development progresses, the *Zic2*$^{Ku/Ku}$ mutants can be further distinguished from their wild type and heterozygous littermates. At E11.5, *Zic2*$^{Ku/Ku}$ mutants are visibly smaller than *Zic2*$^{+/+}$ and *Zic2*$^{Ku/+}$ embryos (*cf*. Figure 3-5C and Figure 3-5A, 3-5B). In addition, all mutants have an open neural tube (arrowheads in Figure 3-5C; larger view of caudal neural tube defect in Figure 3-5C', larger view of exencephaly in the hindbrain in Figure 3-5C'') and some

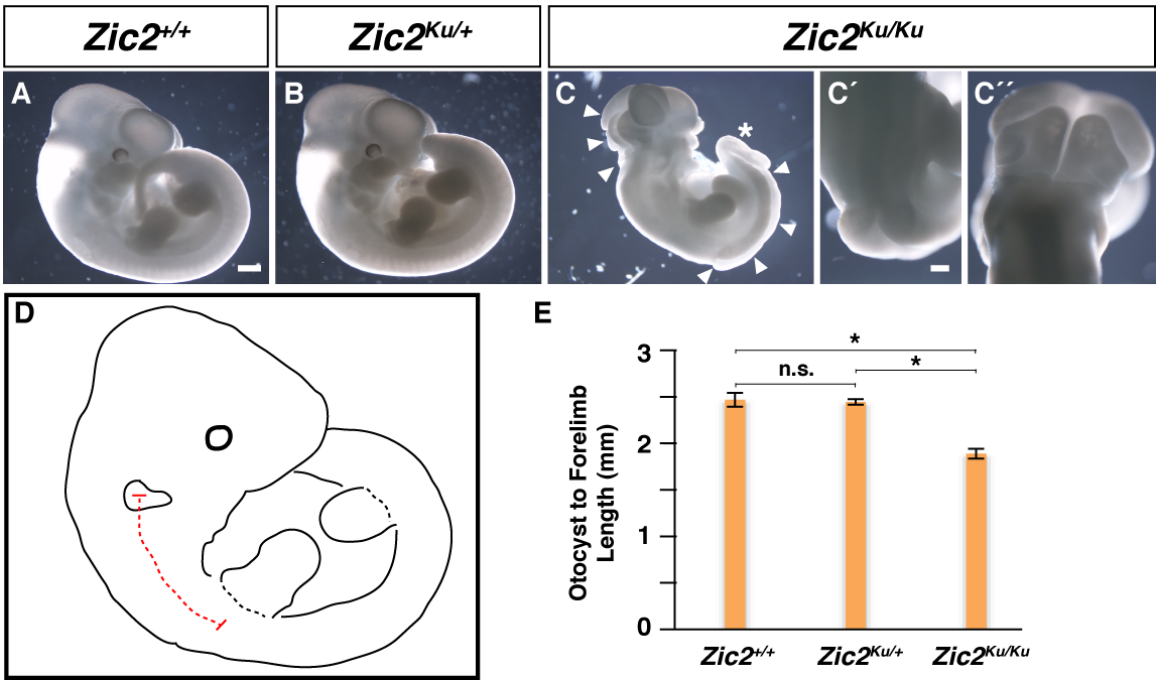

Figure 3-5. Gross Morphology of *Zic2*^{Kumba} Embryos at E11.5. Although *Zic2*$^{+/+}$ (A) and *Zic2*$^{Ku/+}$ (B) embryos show no gross morphological defects at E11.5, the *Zic2*$^{Ku/Ku}$ embryos (C-C'') are smaller than both their *Zic2*$^{+/+}$ and *Zic2*$^{Ku/+}$ littermates, have severe defects in the hindbrain and caudal regions of the neural tube (arrowheads in C), and display a kinked tail (asterisk in C). Higher magnification images show failure of the caudal neural tube to close (C') and exencephaly in the hindbrain (C''). The trunk length of the embryos from the midpoint of the otocyst to the midpoint of the forelimb was measured as shown in (D) and compared among the three genotypes (E; n=6 for each genotype). p-values are designated as follows: *, p<0.0001; n.s., not significant. Error bars in E represent the SEM. Scale bar in A, 500μm (applies to panels A-C); scale bar in C' , 200μm (applies to panels C'-C''). **[n=6 for each genotype]**

---

display a kinked or bent tail (asterisk in Figure 3-5C). To quantify the size difference between the mutants and their littermates, we measured along the neural tube from middle of the otocyst to the middle of the forelimb and compared these distances among the three genotypes (schematic in Figure 3-5D). The *Zic2*$^{Ku/Ku}$ mutants had a significantly shorter otocyst-to-forelimb distance compared to either wild type or heterozygous littermates (Figure 3-5E). We found

no difference in somite numbers among the *Zic2*$^{+/+}$, *Zic2*$^{Ku/+}$, or *Zic2*$^{Ku/Ku}$ embryos, indicating that the shortened otocyst-to-forelimb distance could not be due to defects in somitogenesis. Instead, the shortened distance likely results from defects in the specification of segments along the neural tube. Consistent with this explanation, previous work found that rhombomeres 3 and 5 were smaller in the *Zic2*$^{Ku/Ku}$ mutants, indicating that this may at least partially explain the shortened otocyst-to-forelimb distance (Elms, Siggers et al. 2003).

One day later at E12.5 (Figure 3-6), the accumulated neural tube closure defects cause the *Kumba* mutants to look nothing like either the *Zic2*$^{+/+}$ or *Zic2*$^{Ku/+}$ embryos. *Zic2*$^{Ku/Ku}$ embryos are smaller than their littermates and have open neural tubes in both caudal and rostral regions (*cf*. Figure 3-6C and Figure 3-6A, 3-6B; arrowheads in Figure 3-6C denote regions of open neural tube). At higher

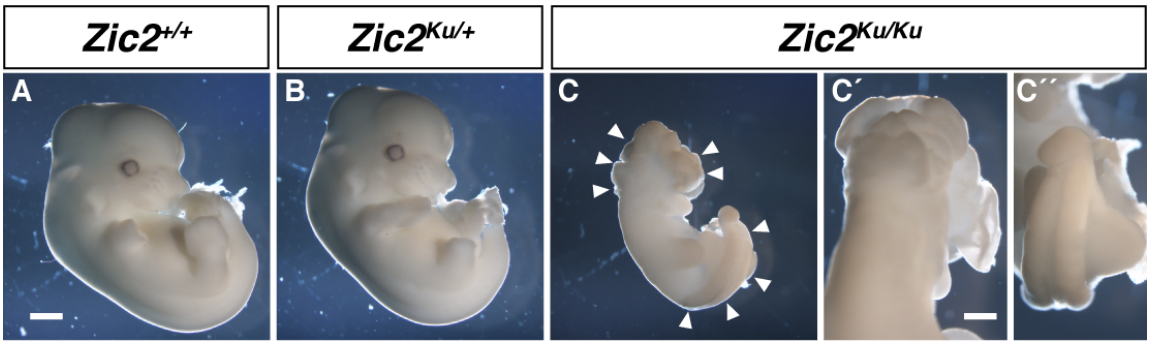

Figure 3-6. Gross Morphology of *Zic2*^{Kumba} Embryos at E12.5. *Zic2*$^{+/+}$ (A) and *Zic2*$^{Ku/+}$ (B) embryos show no gross morphological defects at E12.5. However, *Zic2*$^{Ku/Ku}$ embryos (C-C'') are smaller than both their *Zic2*$^{+/+}$ and *Zic2*$^{Ku/+}$ littermates and have severe defects in the forebrain, hindbrain, and caudal regions of the neural tube (arrowheads in C). Higher magnification images show exencephaly in the hindbrain (C') and spina bifida in the caudal neural tube (C''). Scale bar in A, 1000μm (applies to panels A-C); scale bar in C', 500μm (applies to panels C'-C''). **[n=2 for each genotype]**

magnifications, exencephaly in the hindbrain (Figure 3-6C'), spina bifida in the caudal neural tube (Figure 3-6C''), and a kinked tip of the tail (Figure 3-6C'') can be seen more clearly.

Altered Positioning of Otocyst Relative to the Hindbrain in *Zic2*$^{Ku/Ku}$ Mutants

Inner ears from the *Zic2*$^{Ku/Ku}$ mice were abnormally positioned relative to the neural tube compared to those from wild type mice. The extent of these neural tube closure defects varied from mutant to mutant. The positional abnormalities (Figure 3-7A) included tilting of the ears so that the dorsal-ventral axis of the otocyst was now oriented in a dorso-lateral to ventro-medial direction (TILTED), curling of the open neural tube around the upper portion of the otocyst (CURL-OVER), an increase in the distance between the otic epithelium and the neural tube (SEPARATED), and abnormally shaped otocysts (ALTERED SHAPE). Neural tube closure defects varied and could be classified into distinct types (Figure 3-7B), including open neural tube (Type I), open neural tube that curled (Type II), and neural tube that improperly closed (Type III). As a result of these positional changes between the hindbrain and otocyst, we reasoned that otocyst patterning could be affected, leading to the inner ear phenotypes we observed.

Otocyst Patterning is Unaffected in the *Zic2*$^{Ku/Ku}$ Mutants

Cells in the otic epithelium integrate multiple signals, especially from the SHH, WNT, and BMP pathways leading to regionalized gene expression in the otic epithelium. We looked at the expression of a number of these genes that are

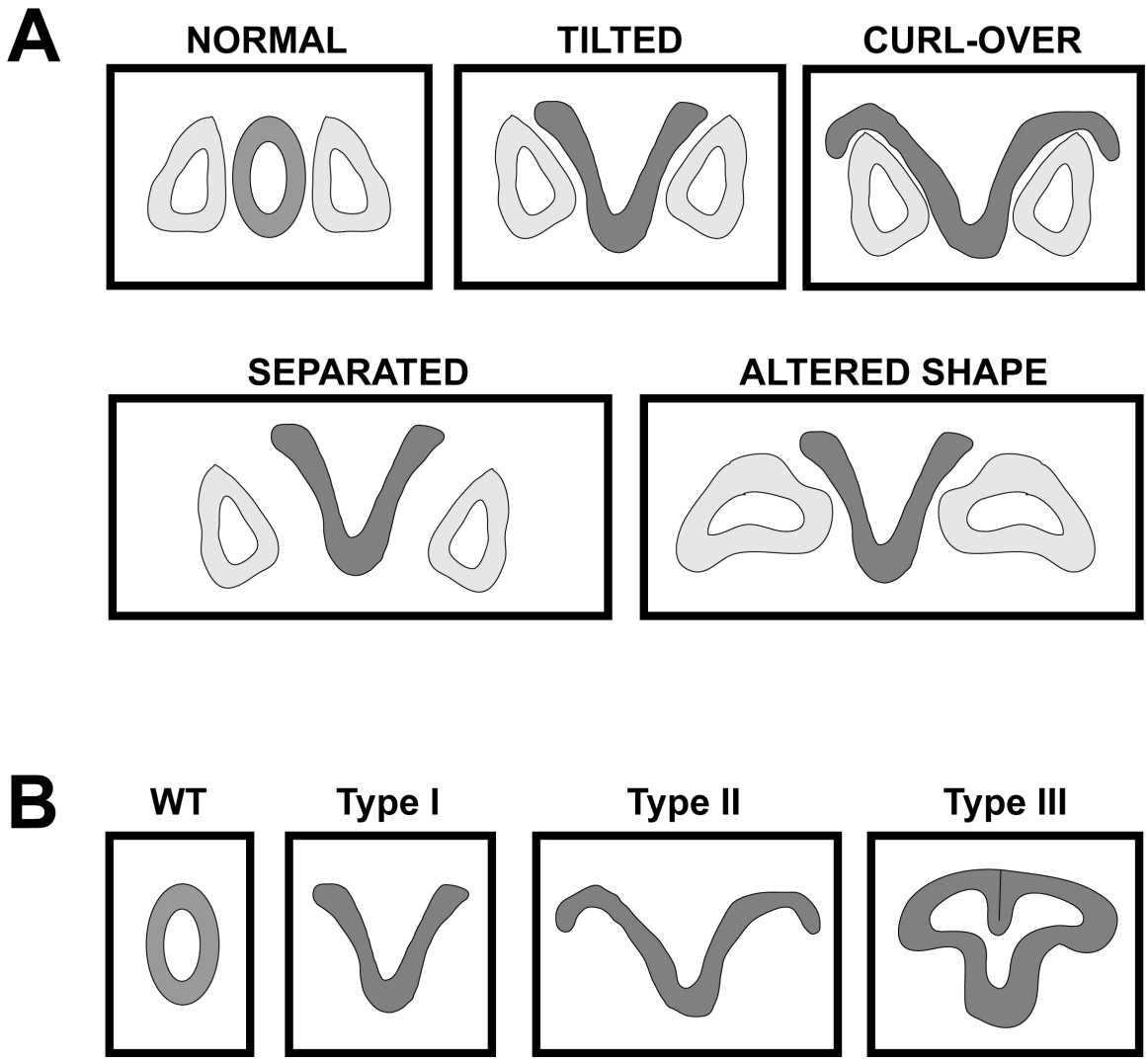

Figure 3-7. Variability of the Inner Ear Phenotypes in *Zic2*$^{Ku/Ku}$ Mice. (A) Variations observed in the shape and position of the otocyst relative to the neural tube in the *Zic2*$^{Ku/Ku}$ mutants. (B) Variations observed in the extent of neural tube closure defects in the *Zic2*$^{Ku/Ku}$ mutants.

---

regulated by WNT, SHH, and BMP signaling and that are expressed in specific regions of the otic epithelium to determine if their expression changed as a result of *Zic2* loss.

We first looked at the expression of *Pax2* (Figure 3-8), one of the first genes expressed in the otic epithelium and one that is positively regulated by SHH signaling and partially restricted by WNT and BMP signals from the dorsal hindbrain (Riccomagno, Martinu et al. 2002; Riccomagno, Takada et al. 2005). *Pax2* expression was unchanged in the otic epithelium of the *Zic2*$^{Ku/Ku}$ mutants at E9.5, E10.5, and E12.5 when compared to inner ears from *Zic2*$^{+/+}$ and *Zic2*$^{Ku/+}$ littermates (*cf*. Figure 3-8A, D, G and Figure 3-8B, E, H, Figure 3-8C, F, I; Supplemental Figures 1-3).

We then examined the expression of *Dlx5*, *Gbx2,* and *Lfng* in the otic epithelium of *Zic2*$^{Ku/Ku}$ mutants (Figure 3-9; Supplemental Figures 4-9). *Dlx5* expression is negatively regulated by SHH signaling and positively regulated by WNT signaling, *Gbx2* expression is positively regulated by both SHH and WNT signaling, and *Lfng* is a SHH-responsive gene whose expression shifts in the absence of *Shh* (Riccomagno, Martinu et al. 2002; Riccomagno, Takada et al. 2005). *Dlx5* expression levels in the mutants did not change at either E9.5 (Supplemental Figure 4) or E10.5 (Figure 3-9A-C, Supplemental Figure 5), however the exact region of expression of *Dlx5* in the otic epithelium of the *Zic2*$^{Ku/Ku}$ embryos appeared to shift, and this shift corresponded to the degree to which the position of the otocyst itself was shifted (*cf*. Figure 3-9C and Figures 3-9A, 3-9B; Supplemental Figures 4 and 5). As the otocyst tilted laterally, the *Dlx5*-expressing region also shifted relative to its normal position in wild type ears, giving the appearance that the expression domain had shifted laterally when in fact it did not shift relative to its normal position within the otocyst.

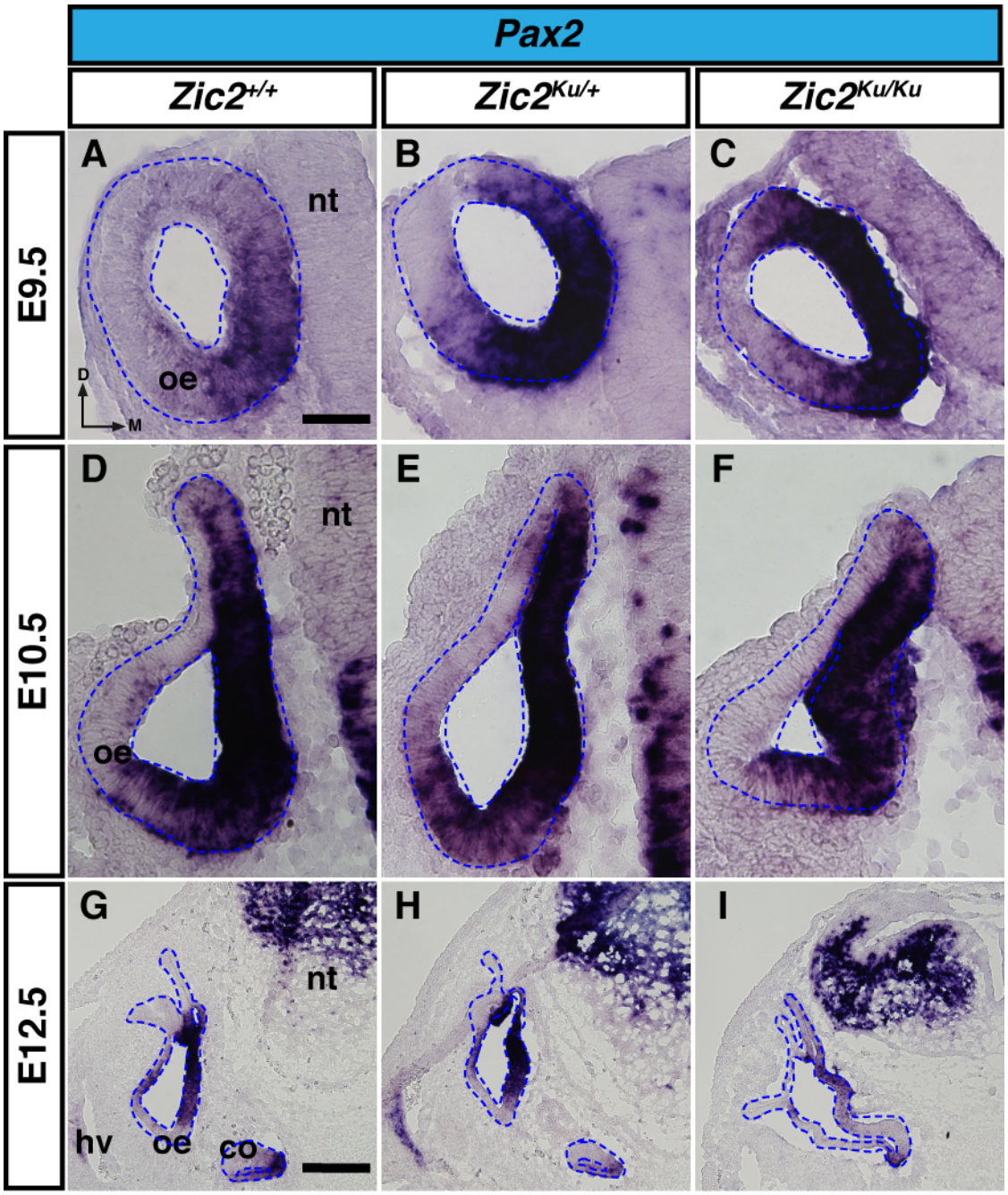

Figure 3-8. Comparison of *Pax2* Expression in the Developing Inner Ear in the *Zic2*^{Ku} Mouse Model. *In situ* hybridization using a probe for *Pax2* was performed on sections through the inner ear region of *Zic2*$^{+/+}$ (A, D, G), *Zic2*$^{Ku/+}$ (B, E, H), and *Zic2*$^{Ku/Ku}$ (C, F, I) embryos at E9.5 (A-C), E10.5 (D-F), and E12.5 (G-I). Blue dashed lines outline the otic epithelium. Abbreviations: oe, otic epithelium; nt, neural tube; co, cochlea; d, dorsal; m, medial. Scale bar in A, 50μm (applies to A-F); scale bar in G, 200μm (applies to G-I). **[E9.5: n=1 for all genotypes; E10.5: n=2 (*Zic2*$^{+/+}$, *Zic2*$^{Ku/+}$), n=3 (*Zic2*$^{Ku/Ku}$); E12.5: n=1 for all genotypes]**

Expression of *Gbx2* was detected in the dorso-medial region of the otic epithelium in *Zic2*$^{Ku/Ku}$ mutants at E9.5, which was the same pattern observed in the otic epithelium of both *Zic2*$^{+/+}$ and *Zic2*$^{Ku/+}$ embryos (Supplemental Figure 6). At E10.5, the extent and location of expression of *Gbx2* in *Zic2*$^{Ku/Ku}$ mutant embryos did not differ from that of *Zic2*$^{+/+}$ and *Zic2*$^{Ku/+}$ embryos (cf. Figure 3-9F and Figures 3-9D, Figure 3-9E; Supplemental Figure 7).

The level of expression of *Lfng* in the otic epithelium was unchanged among inner ears from *Zic2*$^{+/+}$, *Zic2*$^{Ku/+}$, and *Zic2*$^{Ku/Ku}$ embryos at both E9.5 (Supplemental Figure 8) and E10.5 (Figure 3-9G-I, Supplemental Figure 9). The region of expression did appear to change relative to that found in *Zic2*$^{Ku/+}$ and *Zic2*$^{Ku/Ku}$ embryos, but this apparent change was due to the malformation of the neural tube and the delay in outgrowth from the dorsal portion of the otocyst. The open neural tube displaced the otocyst laterally, causing the region of *Lfng* expression to appear to have shifted laterally. If the otocyst were tilted medially back into its normal positioning relative to the D-V axis, the region of *Lfng* expression would be indistinguishable from that found in otocysts from wild type mice. *Lfng* expression appears to be more extensive in the otocyst in *Zic2*$^{Ku/Ku}$ mice (*cf*. Figure 3-9I and Figure 3-9G, 3-9H). Since the outgrowth of the endolymphatic duct is delayed in the ears of *Zic2*$^{Ku/Ku}$ mice (Figure 3-3C), this apparent expansion of expression can be explained by the delay in the dorsal outgrowth of the otic epithelium.

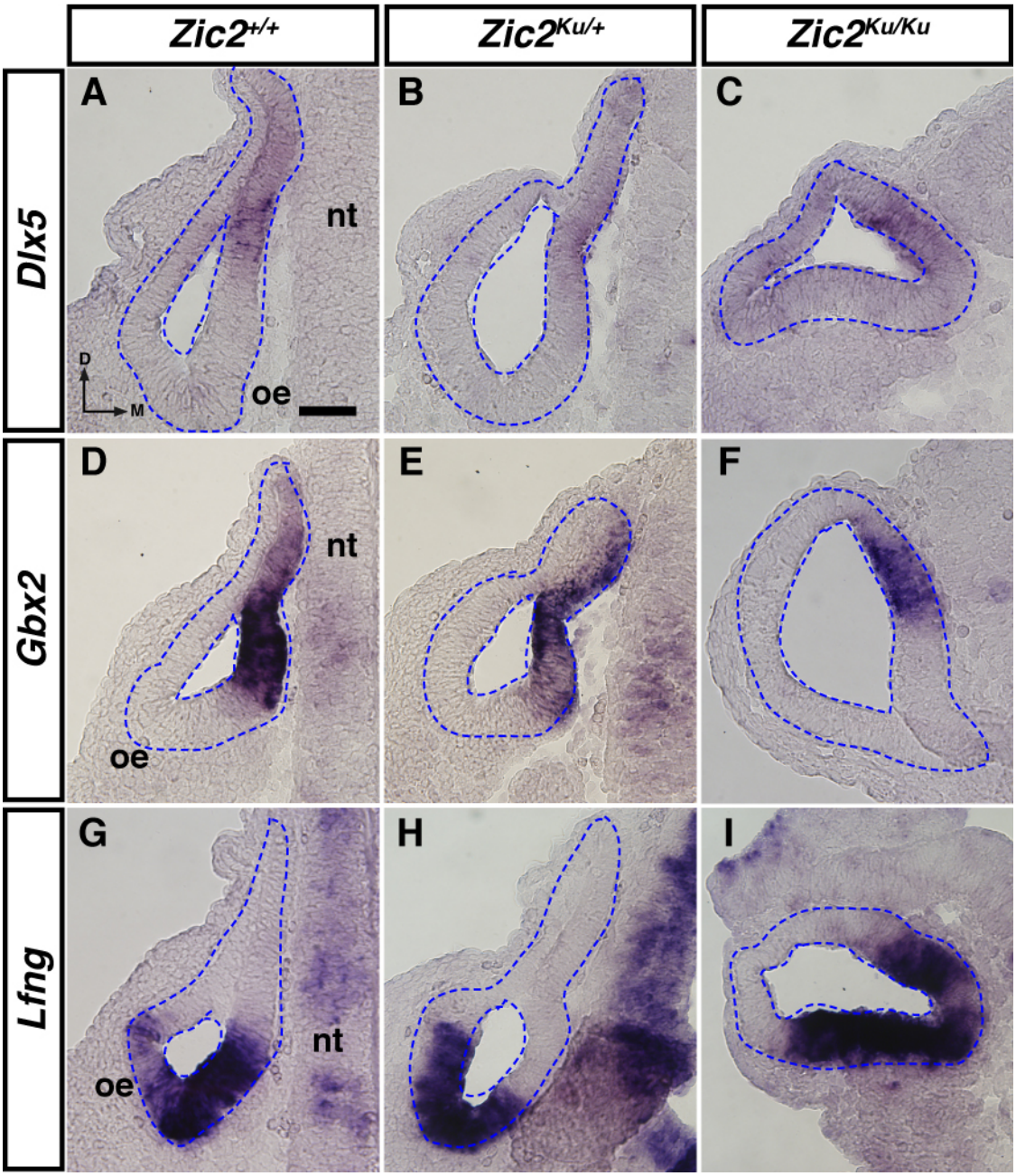

Figure 3-9. Comparison of *Dlx5*, *Gbx2*, and *Lfng* Expression in the Developing Inner Ear at E10.5 in the *Zic2*^{Ku} Mouse Model. *In situ* hybridization using probes for *Dlx5* (A-C), *Gbx2* (D-F), and *Lfng* (G-I) were performed on sections through the inner ear region of *Zic2*$^{+/+}$ (A, D, G), *Zic2*$^{Ku/+}$ (B, E, H), and *Zic2*$^{Ku/Ku}$ (C, F, I) embryos. Blue dashed lines outline the otic epithelium. Abbreviations: oe, otic epithelium; nt, neural tube; d, dorsal; m, medial. Scale bar in A, 50μm (applies to A-I). **[n=3 for all genes and all genotypes]**

Expression of Mesenchymal Genes Relatively Unchanged in *Zic2*$^{Ku/Ku}$ Mutants

We noticed that in the *Zic2*$^{Ku/Ku}$ mutants, there was an increase in the distance between the neural tube and the otocyst, and that this increase in distance corresponded to an increase in the number of cells observed between these two structures. We looked at the expression of *Tbx1* and *Brn4* to determine if these cells were periotic mesenchyme cells or regions of condensing cartilage as we had previously done in our earlier study (Chervenak, Hakim et al. 2013). The changed position of the otocyst relative to the sources of WNT and SHH signals may have affected the expression of *Tbx1* and *Brn4*, two genes that are regulated by WNT and SHH signaling (Riccomagno, Martinu et al. 2002; Riccomagno, Takada et al. 2005). *Tbx1* is normally expressed in the dorso-lateral half of the otic epithelium and in the mesenchyme between the neural tube and otic epithelium, as well as in the mesenchyme adjacent to the ventral otic epithelium. This expression pattern was found in inner ears from *Zic2*$^{+/+}$, *Zic2*$^{Ku/+}$, and *Zic2*$^{Ku/Ku}$ embryos at E9.5 (Supplemental Figure 10) and E10.5 (Supplemental Figure 11). In *Zic2*$^{Ku/Ku}$ embryos, the larger number of cells found between the neural tube and the developing inner ear was *Tbx1*+, indicating that these are periotic mesenchyme cells. Based on these limited experiments, it could not be determined whether this increase was due to increased proliferation of periotic mesenchyme cells or a result of periotic mesenchyme cells being displaced due to the severe morphological defects of these embryos. *Brn4* expression at E9.5 and E10.5 appeared to be unchanged in the *Zic2*$^{Ku/Ku}$

mutants, indicating no apparent changes in the regions of condensing cartilege (Supplemental Figure 12).

3.4. Discussion

The Loss of *Zic1* and *Zic4* May Be Compensated for by Other *Zic* Genes

Zic1 and *Zic4* have been shown to have redundant functions in cerebellar development, as loss of either *Zic1* or *Zic4* alone has a milder phenotype as compared to a *Zic1*/*Zic4* double mutant (Aruga, Minowa et al. 1998; Grinberg, Northrup et al. 2004; Blank, Grinberg et al. 2011). When we analyzed the morphology of inner ears from *Zic1*$^{-/-}$;*Zic4*$^{-/-}$ embryos, we did not observe any obvious gross morphological defects in the size or shape of the developing inner ears through E15.5, the last stage examined. It is possible that *Zic1* and *Zic4* are involved in later development of the inner ear, such as in the development and maturation of the sensory patches. More likely, however, is that other *Zic* genes have redundant roles and can compensate for the loss of *Zic1* and *Zic4*, as the expression of *Zic1* and *Zic4* overlap in the dorso-medial periotic mesenchyme in a region in which both *Zic2* and *Zic3* are also expressed in the developing inner ear in chick and mouse (Chervenak, Hakim et al. 2013).

Zic2 Is Important for Inner Ear Development in Mouse

During the initial stages of inner ear development in the mouse, *Zic2* is expressed in the dorsal hindbrain and in the mesenchyme adjacent to the otic epithelium (Chervenak, Hakim et al. 2013). The extent of expression of *Zic2* in

the mesenchyme expands in a dorsal to ventral wave between E9.5 and E11.5, with expression initially restricted to the dorsal and medial periotic mesenchyme at E9.5 (Chervenak, Hakim et al. 2013). By E13.5, when the ear has undergone the majority of its morphological changes to adopt its characteristic three dimensional form, with extended endolymphatic duct and sac, 3 fused semicircular canals and coiling cochlear duct (see Figure 3-2C for an example), *Zic2*-expressing periotic mesenchyme cells completely surround the otic epithelium (Chervenak, Hakim et al. 2013). In light of these recent expression data, the results of the earlier study in chick indicating that *Zic2* was upregulated after noise trauma may actually reflect upregulation of *Zic2* in the periotic mesenchyme and not the otic epithelium, leading us to speculate that *Zic2* has no ***direct*** role in a sensory cell or supporting cell-transdifferentiative regenerative response (reviewed in Stone and Cotanche 2007). Therefore, since *Zic2* is more globally expressed throughout the periotic mesenchyme compared to the other *Zic* genes, and given the redundant expression of *Zic1*/*Zic4*, we hypothesized that loss of *Zic2* would result in morphological inner ear defects in the mouse.

Indeed, either partial ($Zic2^{kd/kd}$) or complete loss ($Zic2^{Ku/Ku}$) of *Zic2* resulted in significant defects in inner ear morphology. In the $Zic2^{kd/kd}$ inner ears, both dorsal (vestibular) and ventral (cochlea) structures were severely affected, which was notable by E13.5. Defects in the inner ears of $Zic2^{Ku/Ku}$ mice were seen earlier, starting at E11.5, and likely reflect the effects of total loss of *Zic2* compared to partial loss in the $Zic2^{kd/kd}$ mice. Inner ears from $Zic2^{Ku/Ku}$ mice exhibited delayed outgrowth of both the endolymphatic sac and endolymphatic

and cochlear ducts, and ears were noticeably smaller than wild type ears at both E11.5 and E12.5 (Figure 3-3). We could not compare inner ears from the *Zic2*$^{Ku/Ku}$ and *Zic2*$^{kd/kd}$ mice past E12.5 due to the embryonic lethality caused by the homozygous loss of *Zic2*, so we cannot determine if the total loss of *Zic2* has different effects on inner ear development, or if it accelerates the onset of the same defects seen in the *Zic2*$^{kd/kd}$ mice.

Function of *Zic2* During Inner Ear Development

Both *Zic2*$^{kd/kd}$ and *Zic2*$^{Ku/Ku}$ mutants have neural tube closure defects in the hindbrain region, and in *Zic2*$^{Ku/Ku}$ mutants, rhombomeres 3 and 5 (r3, r5) are smaller than those in wild type embryos (Nagai, Aruga et al. 2000; Elms, Siggers et al. 2003). These neural tube closure defects affect the positioning of the otocyst relative to the hindbrain, and thus may also affect the WNT, BMP, and SHH signals from the hindbrain to the otocyst, resulting in altered patterning of the otocyst. The extent of these neural tube-generated signals' "reach" and therefore influence on the developing inner ear would diminish as the position of the inner ear with respect to the hindbrain was altered. There is a report in the literature that the hindbrain and the inner ear are gap-junction coupled early in inner ear development (Jungbluth, Willecke et al. 2002). Changes in proximity of the inner ear to the hindbrain could therefore drastically influence the ability of hindbrain-generated small molecular weight signals to reach the otic epithelium.

In the most severely affected *Zic2*$^{Ku/Ku}$ mutants, the neural tube in the hindbrain region was splayed open and the inner ears were displaced laterally

(Figure 3-12). However, the position of the inner ear relative to the floor plate and notochord, sources of SHH signaling, was unchanged. Not surprisingly, the expression of SHH-responsive genes in the mesenchyme (*Tbx1*, *Brn4*) and in the otic epithelium (*Lfng*, *Pax2*, *Tbx1*, *Gbx2*) was unchanged. Similarly, the positioning of the inner ear relative to the dorsal hindbrain, source of WNT signaling, was also unchanged in $Zic2^{Ku/Ku}$ mutants, and expression of the WNT-responsive genes *Gbx2* and *Dlx5* was also unaffected. Taken together, these data suggest that loss of *Zic2* does not affect patterning of the otocyst.

In addition to being expressed in the dorsal neural tube, however, *Zic2* is also expressed in the periotic mesenchyme surrounding the inner ear (Chervenak, Hakim et al. 2013). Since mesenchymal-epithelial interactions are crucial for inner ear development, it is possible that *Zic2* expressed in the periotic mesenchyme is important for these interactions (Braunstein, Monks et al. 2009). The smaller but relatively normal looking inner ears in $Zic2^{Ku/Ku}$ mutants at E12.5 could be the result of a defect in cell proliferation in the otic epithelium itself. In zebrafish, *zic2a* acts downstream of WNT signaling to promote cell proliferation (Nyholm, Wu et al. 2007), so loss of *Zic2* in the periotic mesenchyme could potentially disrupt WNT-mediated proliferation in the otic epithelium. Similarly, *Zic2* could have an opposite role in the periotic mesenchyme, limiting proliferation of these mesenchymal cells. In the cerebellum of both $Zic1^{-/-}$ and $Zic1^{+/-}$;$Zic2^{kd/+}$ mice, cell proliferation in the anterior external germinal layer was reduced, as was the expression of cyclin D1 (Aruga, Minowa et al. 1998; Aruga, Inoue et al. 2002). The $Zic2^{kd/kd}$ mutants, which were only analyzed by paint-fills,

had thickening of inner ear structures that could be caused by an increase in the thickness of the otic capsule due to overgrowth of the periotic mesenchyme (Figure 3-2). Alternatively, low levels of *Zic2* may be required for normal proliferation in the otic epithelium and the periotic mesenchyme but higher levels could be required for proper semicircular canal and cochlea formation, potentially explaining why the inner ears from *Zic2*$^{kd/kd}$ mutants were approximately the same size as those from wild type mice but had malformed (e.g. unfused) or missing semicircular canals and cochleae. If this proves to be the case, then inner ears in mice with complete loss of *Zic2* in the periotic mesenchyme would be expected to resemble those from the *Zic2*$^{kd/kd}$ mutants, but would be smaller due to the combined effects on proliferation and canal formation. However, we could not test this hypothesis in our *Zic2*$^{Ku/Ku}$ mutants, because embryos died shortly after E12.5. Generation of a mouse with a floxed allele of *Zic2* would allow a test of this hypothesis, by making use of the mesenchyme-specific Cre-driver line *Tbx18*^{Cre} to selectively delete *Zic2* in the periotic mesenchyme and analyze inner ear morphology past the stages we were able to study in the *Zic2*$^{Ku/Ku}$ mutants (Trowe, Shah et al. 2010).

Conclusions

Our experiments show that partial or complete loss of *Zic2* affects inner ear development in the mouse. Molecular analysis of inner ear development in *Zic2*$^{Ku/Ku}$ mutants that have a complete loss of *Zic2* show that although hindbrain malformations are present, these do not appear to affect the expression of genes

in the otic epithelium that are regulated by WNT and SHH signaling from the hindbrain. Changes in inner ear morphology in the *Zic2*$^{kd/kd}$ mutants and smaller, misoriented ears in the *Zic2*$^{Ku/Ku}$ mutants suggest that *Zic2* may function to regulate both cell numbers and canal outgrowth during inner ear development, but additional experiments are needed to investigate this further.

3.5. Experimental Procedures

Embedding and Cryosectioning

Embryos were transferred through three progressive changes of OCT (TissueTek) to remove excess sucrose. The embryos were then transferred to embedding molds, covered with OCT, and oriented such that the anterior portion of the ear pointed down. The molds were then frozen on dry ice and stored at -80^{o}C until sectioning. 12μm or 25μm transverse sections through the ear were cut using a Microm HM500M cryostat and collected on SuperFrost Plus slides (Fisher). Sections were air-dried on the slides at room temperature for at least 30 minutes, and then stored at -80^{o}C.

In Situ Hybridization and Immunofluorescence

In situ hybridization using digoxigenin-labeled antisense probes was performed on sections from *Zic2*$^{+/+}$, *Zic2*$^{Ku/+}$, and *Zic2*$^{Ku/Ku}$ embryos as previously described (Chervenak, Hakim et al. 2013). A minimum of 2 embryos was analyzed for each probe. Antisense probes were generated by digesting plasmids containing the cDNA sequences of the genes of interest and then transcribing with the

appropriate RNA polymerase. Immunofluorescence experiments were performed as described previously (Jeong and McMahon 2005). Rabbit anti-mouse α-phospho-Smad1/5/8 antibody (Cell Signaling Technologies) was used at a dilution of 1:200 and detected with AlexaFluor goat anti-rabbit 488 secondary antibody at a dilution of 1:500 (Molecular Probes). Images were acquired with an Olympus BX51 microscope (*in situs*) or a Nikon E-800 microscope (immunofluorescence) equipped with an Olympus camera.

Paint-filling of Inner Ears

Inner ears from *Zic2*^{kd}, *Zic2*^{Kumba}, and *Zic1*/*Zic4* mouse embryos were paint-filled using previously described protocols (Kiernan 2006).

Imaging and Analysis of *Zic2*^{Kumba} Embryos

Whole *Zic2*$^{+/+}$, *Zic2*$^{Ku/+}$, and *Zic2*$^{Ku/Ku}$ embryos and paint-filled inner ears from *Zic2*$^{+/+}$, *Zic2*$^{Ku/+}$, and *Zic2*$^{Ku/Ku}$ embryos were imaged using a Nikon SMZ1500 stereomicroscope and fitted with a Nikon Digital Sight DS-Ri1 camera. The distance from the otocyst to the forelimb and the axial dimensions (anterior-posterior and dorsal-ventral) of the inner ear were measured using NIS Elements D 3.1 software.

3.6. Supplemental Figures

Individual figure legends are included, and the figures are all structured in the same way: wild type (left column), heterozygotes (center column), and mutants (right column); examples clustered by age and/or embryo number into rows starting at the top and moving down. For some genes, all ages fit into one figure while others are split into at least two figures. Each image is oriented the same way, with dorsal to the top. In images displaying only the left ear, lateral is to the left, while in images displaying only the right ear, lateral is to the right.

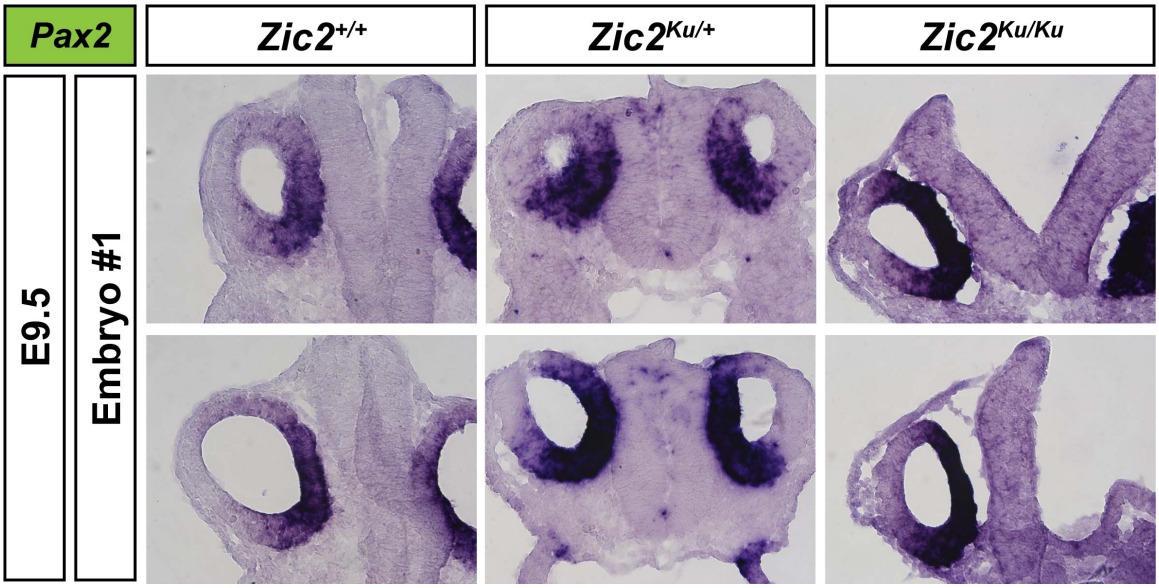

Supplemental Figure 1. *Pax2* expression in the otic region of *Zic2*$^{+/+}$, *Zic2*$^{Ku/+}$, and *Zic2*$^{Ku/Ku}$ mouse embryos at E9.5. *In situ* hybridization on 12µm transverse sections through the otocyst of E9.5 mouse embryos using a probe for *Pax2*. Abbreviations: oe, otic epithelium; nt, neural tube. Blue dashed line outlines the otic epithelium. Top and bottom sections within each embryo cluster ("embryo #1") are from different levels of the ear in the same embryo. **[n=1 for all genotypes]**

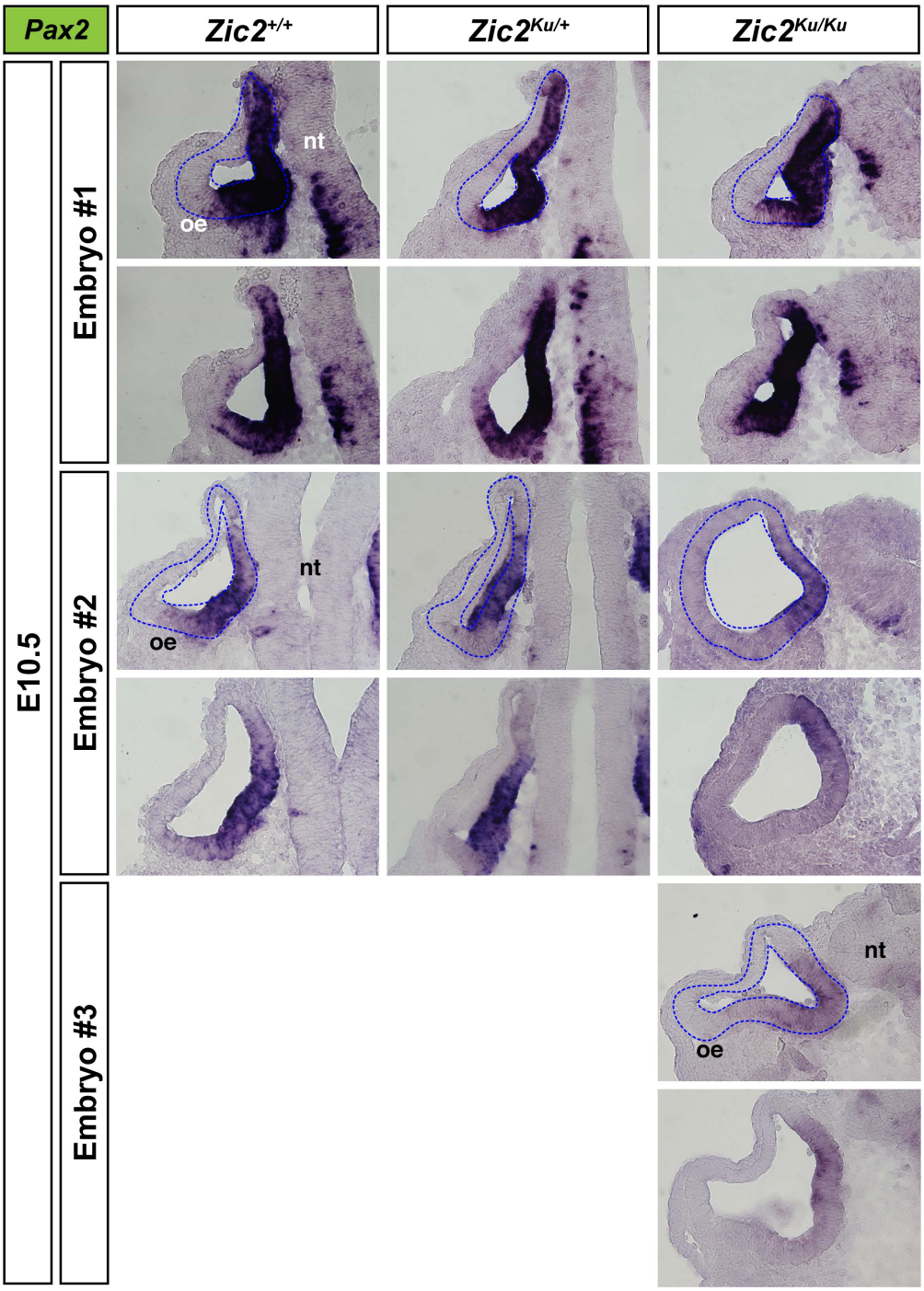

Supplemental Figure 2. *Pax2* expression in the otic region of *Zic2*$^{+/+}$, *Zic2*$^{Ku/+}$, and *Zic2*$^{Ku/Ku}$ mouse embryos at E10.5. *In situ* hybridization on 12µm transverse sections through the otocyst of E10.5 mouse embryos using a probe for *Pax2*. Abbreviations: oe, otic epithelium; nt, neural tube. Blue dashed line outlines the otic epithelium. Top and bottom sections within each embryo cluster ("embryo #1", "embryo #2", "embryo #3") are from different levels of the ear in the same embryo. [**n=2 for *Zic2*$^{+/+}$, *Zic2*$^{Ku/+}$; n=3 for *Zic2*$^{Ku/Ku}$**]

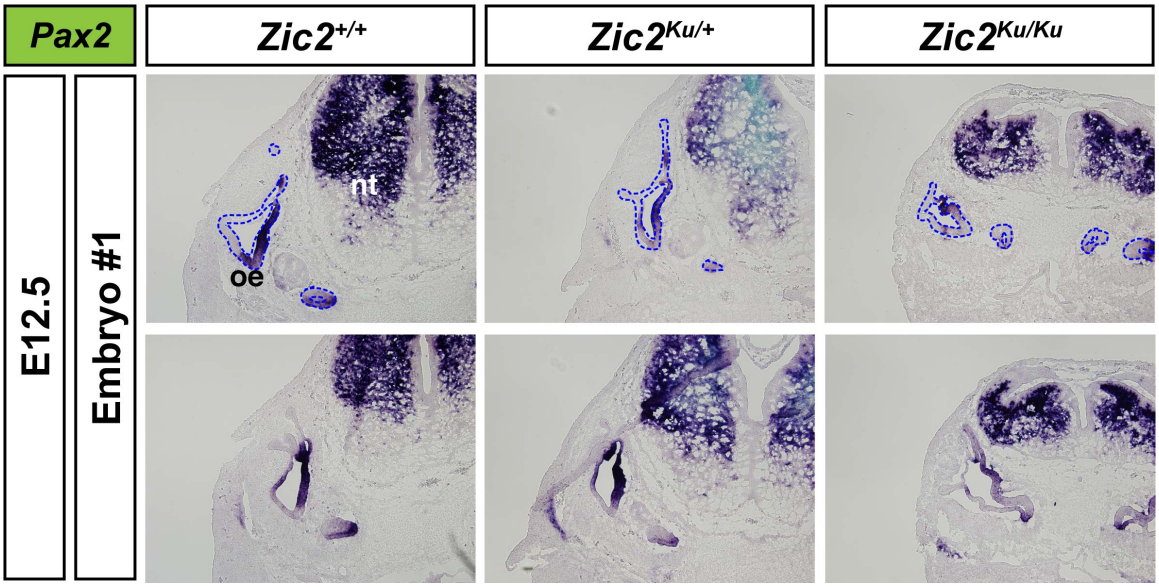

Supplemental Figure 3. *Pax2* expression in the otic region of *Zic2*$^{+/+}$, *Zic2*$^{Ku/+}$, and *Zic2*$^{Ku/Ku}$ mouse embryos at E12.5. *In situ* hybridization on 12µm transverse sections through the otocyst of E12.5 mouse embryos using a probe for *Pax2*. Abbreviations: oe, otic epithelium; nt, neural tube. Blue dashed line outlines the otic epithelium. Top and bottom sections within each embryo cluster ("embryo #1") are from different levels of the ear in the same embryo. **[n=1 for all genotypes]**

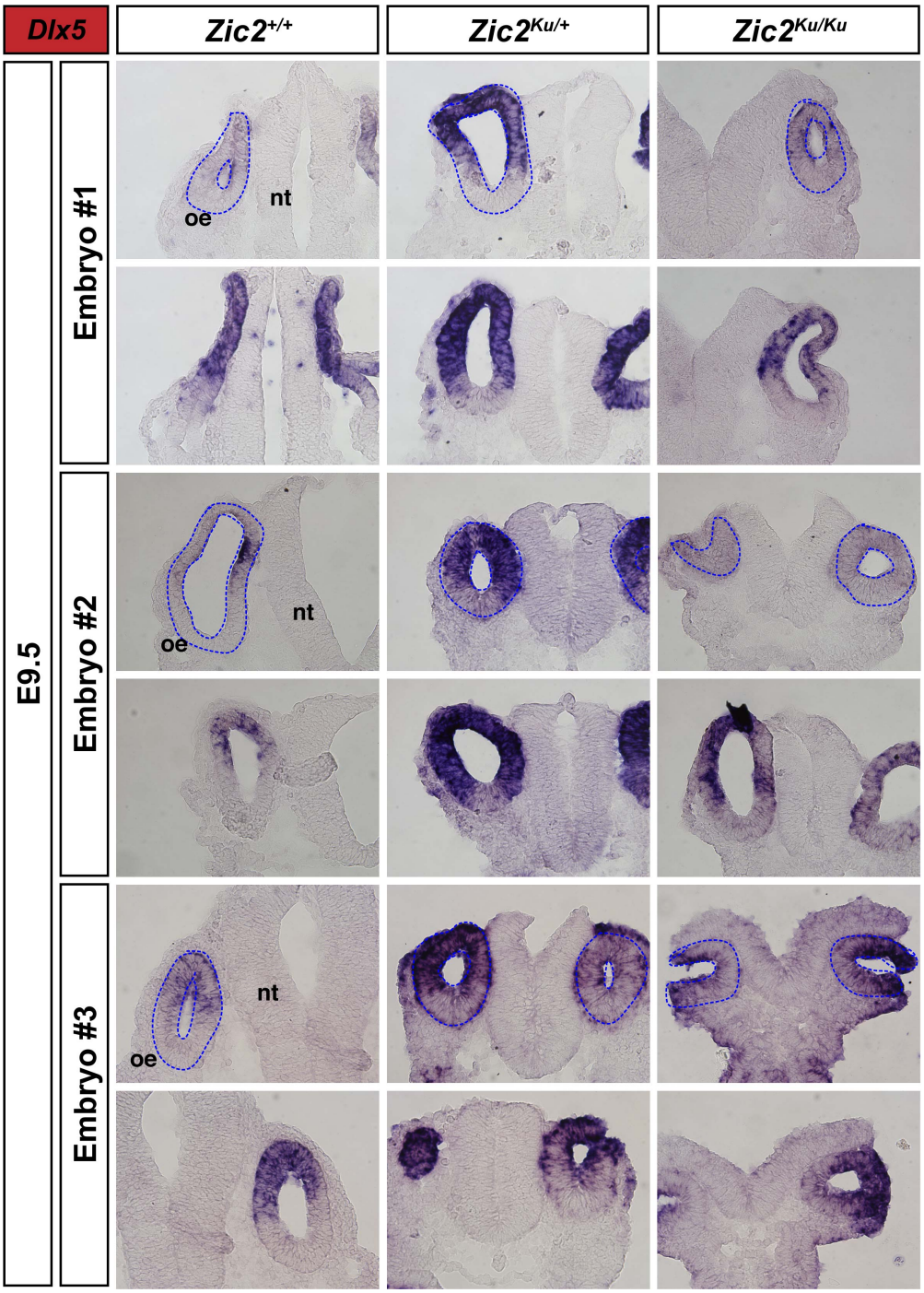

Supplemental Figure 4. *Dlx5* expression in the otic region of *Zic2*$^{+/+}$, *Zic2*$^{Ku/+}$, and *Zic2*$^{Ku/Ku}$ mouse embryos at E9.5. *In situ* hybridization on 12µm transverse sections through the otocyst of E9.5 mouse embryos using a probe for *Dlx5*. Abbreviations: oe, otic epithelium; nt, neural tube. Blue dashed line outlines the otic epithelium. Top and bottom sections within each embryo cluster ("embryo #1", "embryo #2", "embryo #3") are from different levels of the ear in the same embryo. **[n=3 for all genotypes]**

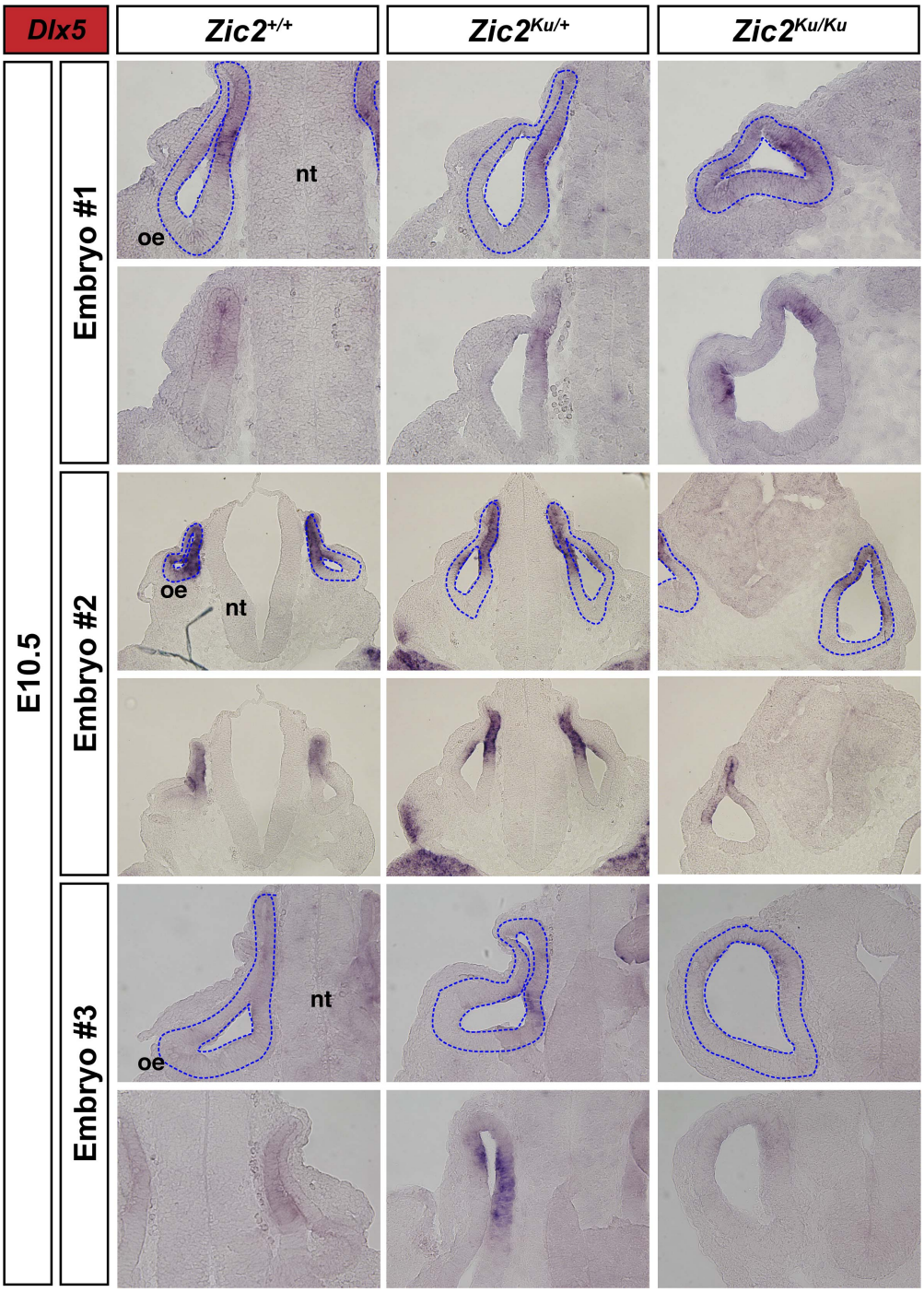

Supplemental Figure 5. *Dlx5* expression in the otic region of *Zic2*$^{+/+}$, *Zic2*$^{Ku/+}$, and *Zic2*$^{Ku/Ku}$ mouse embryos at E10.5. *In situ* hybridization on 12µm transverse sections through the otocyst of E10.5 mouse embryos using a probe for *Dlx5*. Abbreviations: oe, otic epithelium; nt, neural tube. Blue dashed line outlines the otic epithelium. Top and bottom sections within each embryo cluster ("embryo #1", "embryo #2", "embryo #3") are from different levels of the ear in the same embryo. **[n=3 for all genotypes]**

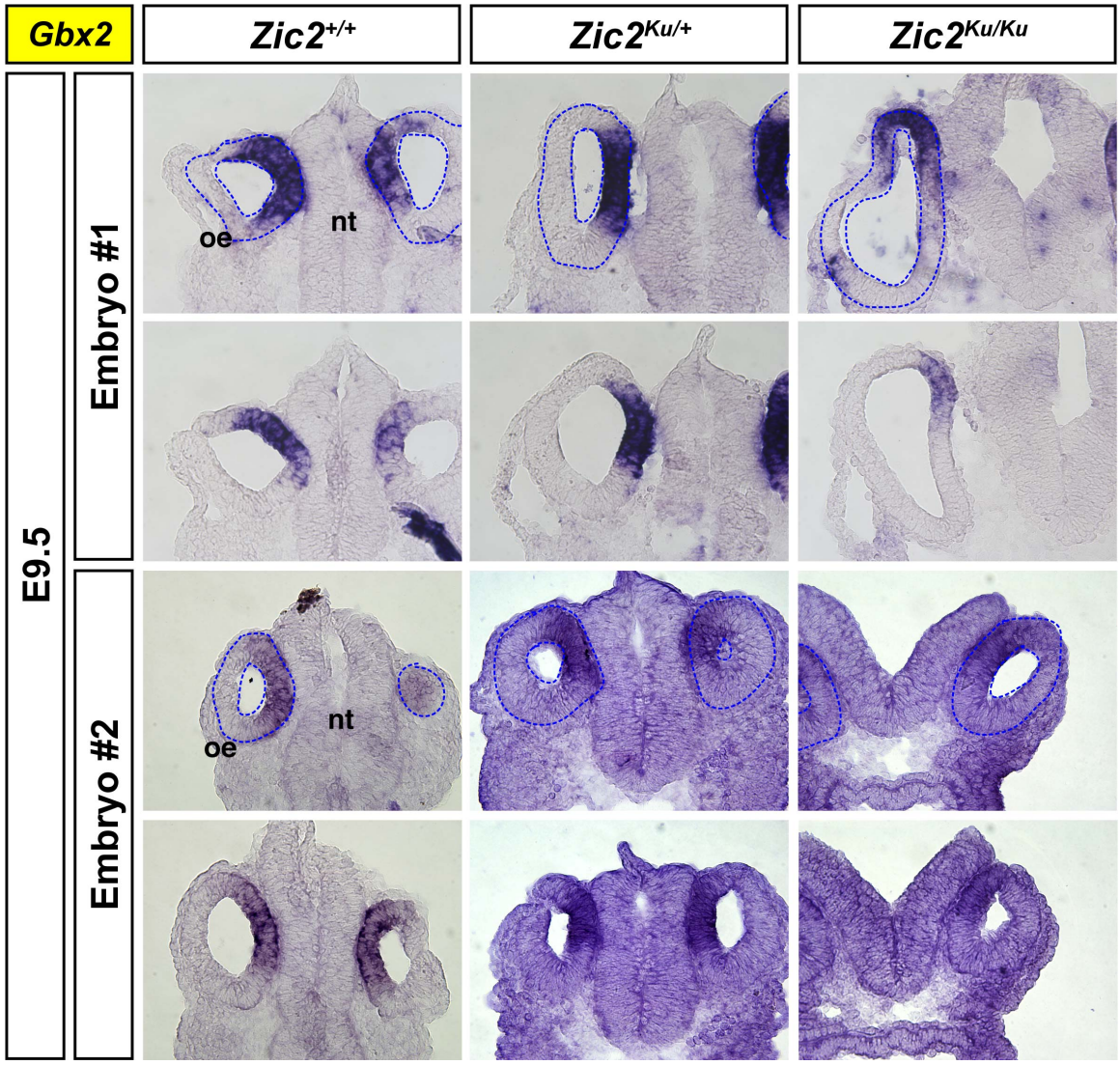

Supplemental Figure 6. *Gbx2* expression in the otic region of *Zic2*$^{+/+}$, *Zic2*$^{Ku/+}$, and *Zic2*$^{Ku/Ku}$ mouse embryos at E9.5. *In situ* hybridization on 12µm transverse sections through the otocyst of E9.5 mouse embryos using a probe for *Gbx2*. Abbreviations: oe, otic epithelium; nt, neural tube. Blue dashed line outlines the otic epithelium. Top and bottom sections within each embryo cluster ("embryo #1", "embryo #2") are from different levels of the ear in the same embryo. **[n=2 for all genotypes]**

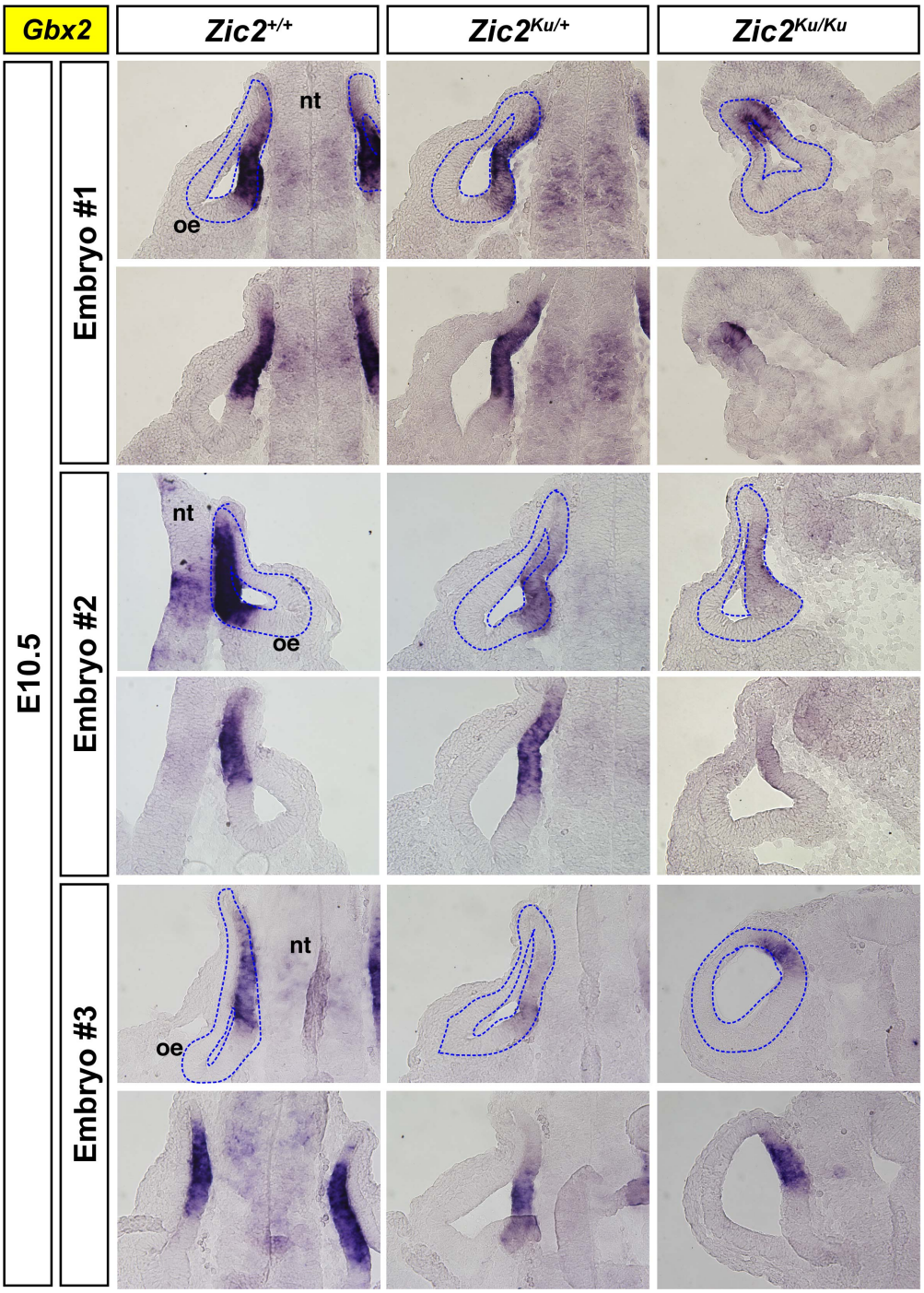

Supplemental Figure 7. *Gbx2* expression in the otic region of *Zic2*$^{+/+}$, *Zic2*$^{Ku/+}$, and *Zic2*$^{Ku/Ku}$ mouse embryos at E10.5. *In situ* hybridization on 12µm transverse sections through the otocyst of E10.5 mouse embryos using a probe for *Gbx2*. Abbreviations: oe, otic epithelium; nt, neural tube. Blue dashed line outlines the otic epithelium. Top and bottom sections within each embryo cluster ("embryo #1", "embryo #2", "embryo #3") are from different levels of the ear in the same embryo. **[n=3 for all genotypes]**

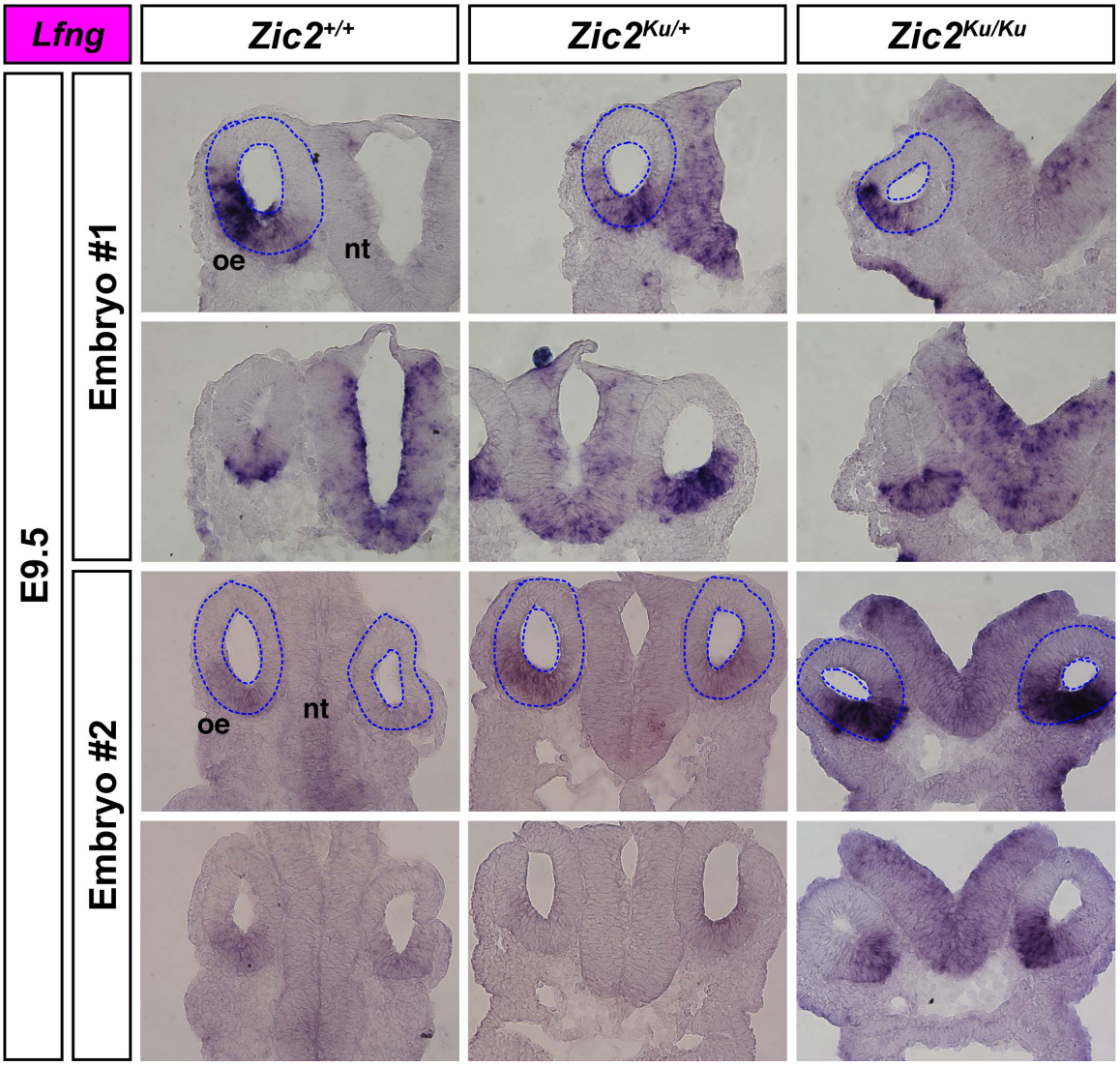

Supplemental Figure 8. *Lfng* expression in the otic region of *Zic2*$^{+/+}$, *Zic2*$^{Ku/+}$, and *Zic2*$^{Ku/Ku}$ mouse embryos at E9.5. *In situ* hybridization on 12µm transverse sections through the otocyst of E9.5 mouse embryos using a probe for *Lfng*. Abbreviations: oe, otic epithelium; nt, neural tube. Blue dashed line outlines the otic epithelium. Top and bottom sections within each embryo cluster ("embryo #1", "embryo #2") are from different levels of the ear in the same embryo. **[n=2 for all genotypes]**

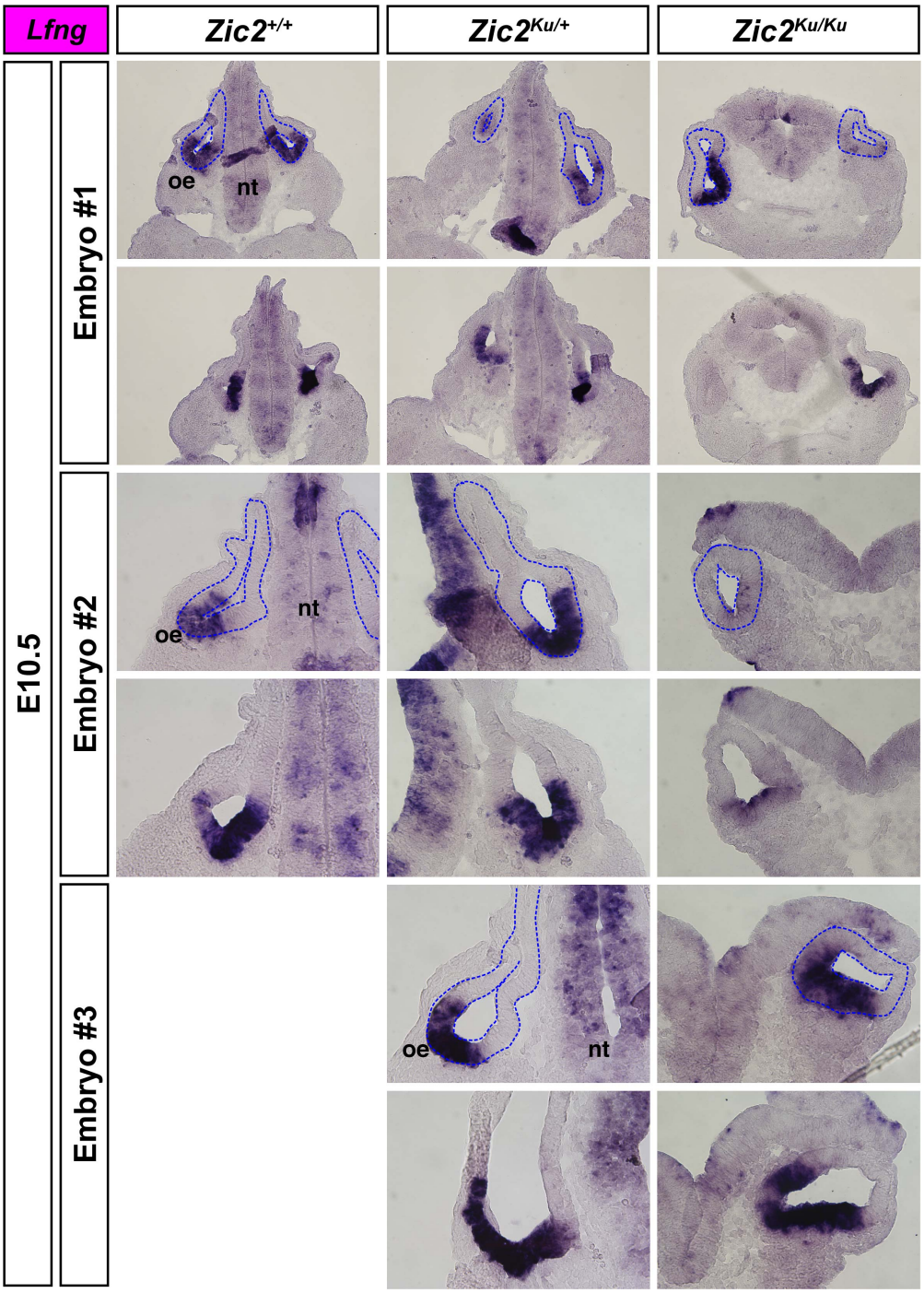

Supplemental Figure 9. *Lfng* expression in the otic region of *Zic2*$^{+/+}$, *Zic2*$^{Ku/+}$, and *Zic2*$^{Ku/Ku}$ mouse embryos at E10.5. *In situ* hybridization on 12µm transverse sections through the otocyst of E10.5 mouse embryos using a probe for *Lfng*. Abbreviations: oe, otic epithelium; nt, neural tube. Blue dashed line outlines the otic epithelium. Top and bottom sections within each embryo cluster ("embryo #1", "embryo #2", "embryo #3") are from different levels of the ear in the same embryo. **[n=2 for *Zic2*$^{+/+}$; n=3 for *Zic2*$^{Ku/+}$ and *Zic2*$^{Ku/Ku}$]**

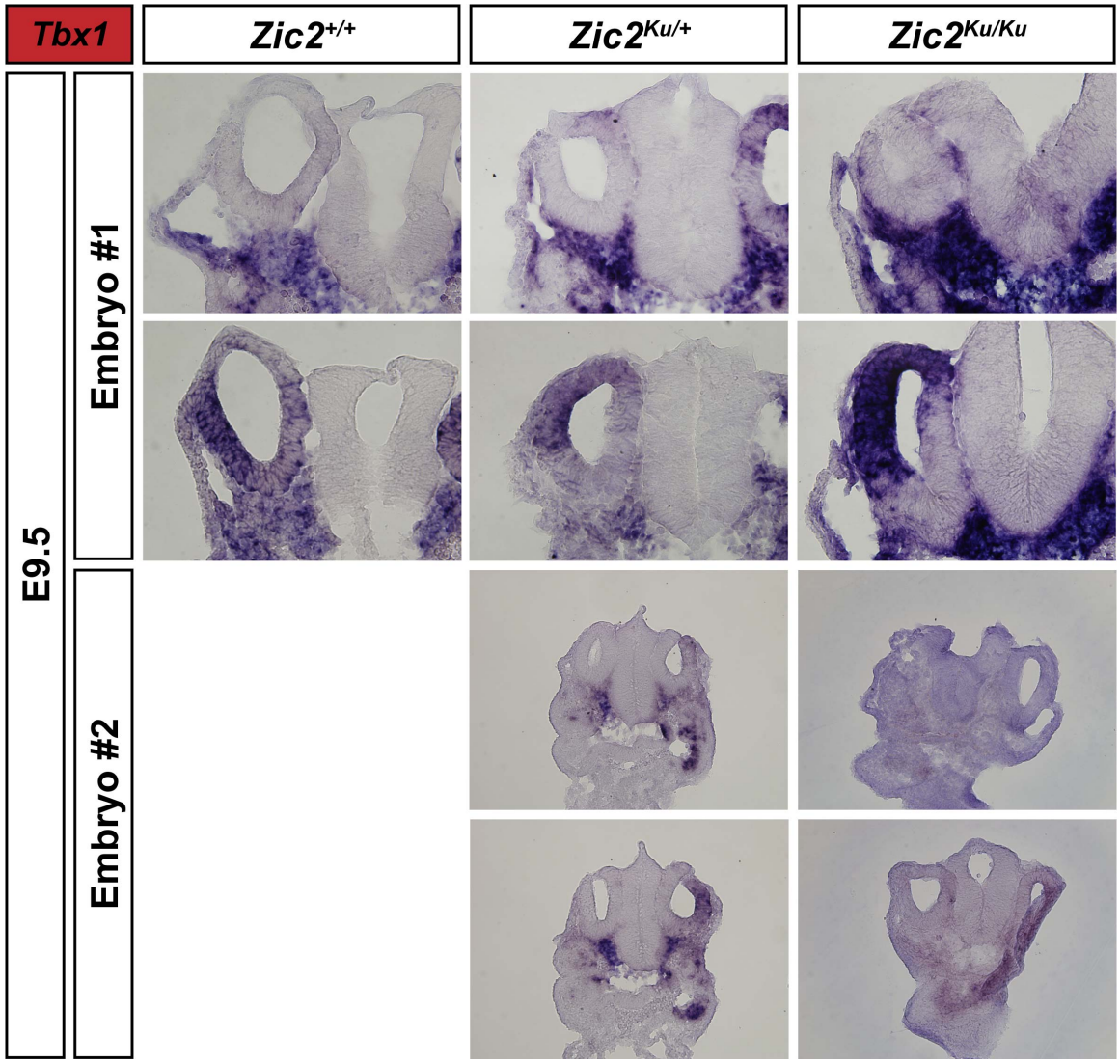

Supplemental Figure 10. *Tbx1* expression in the otic region of *Zic2*$^{+/+}$, *Zic2*$^{Ku/+}$, and *Zic2*$^{Ku/Ku}$ mouse embryos at E9.5. *In situ* hybridization on 12µm transverse sections through the otocyst of E9.5 mouse embryos using a probe for *Tbx1*. Abbreviations: oe, otic epithelium; nt, neural tube. Blue dashed line outlines the otic epithelium. Top and bottom sections within each embryo cluster ("embryo #1", "embryo #2") are from different levels of the ear in the same embryo. **[n=1 for *Zic2*$^{+/+}$; n=2 for *Zic2*$^{Ku/+}$ and *Zic2*$^{Ku/Ku}$]**

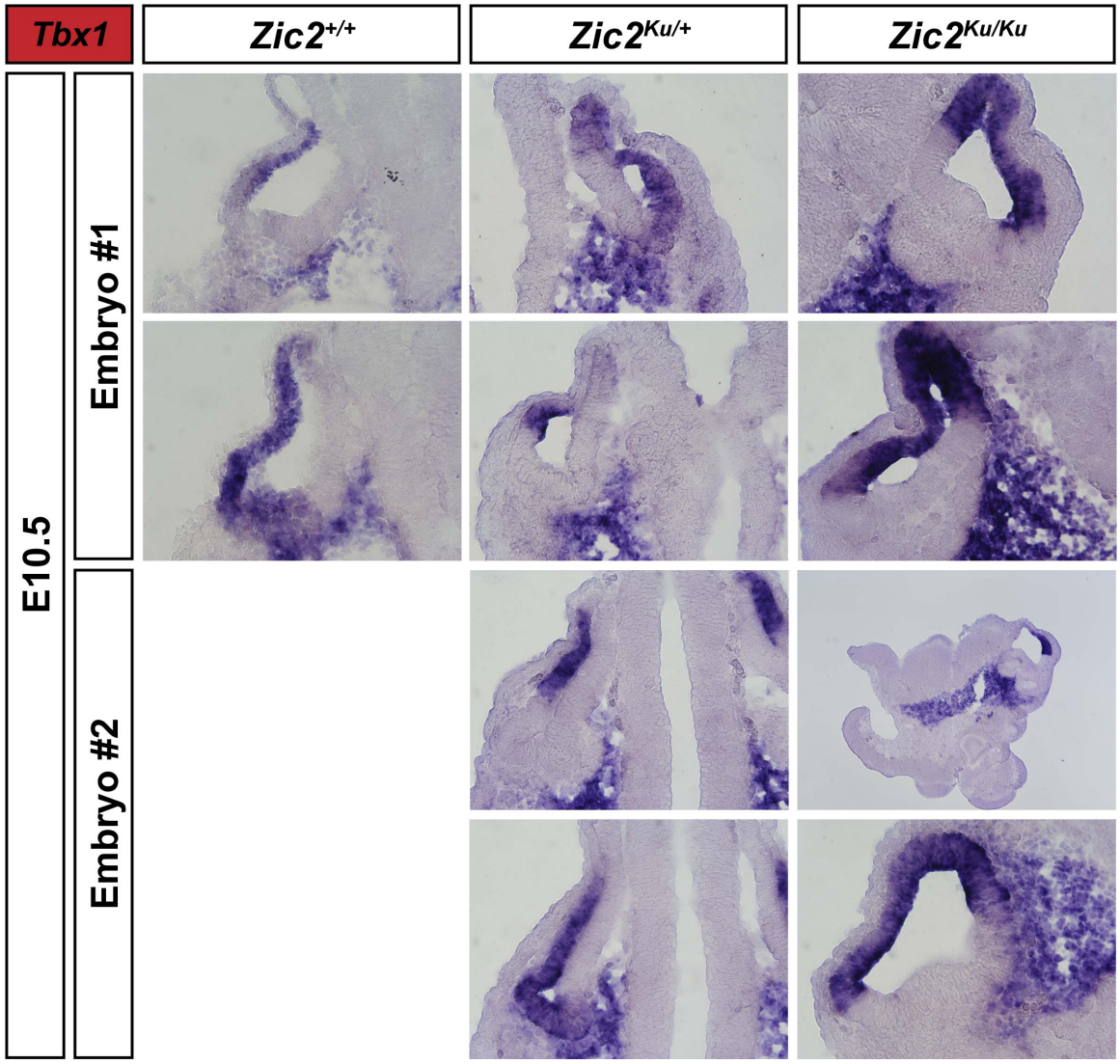

Supplemental Figure 11. *Tbx1* expression in the otic region of *Zic2*$^{+/+}$, *Zic2*$^{Ku/+}$, and *Zic2*$^{Ku/Ku}$ mouse embryos at E10.5. *In situ* hybridization on 12µm transverse sections through the otocyst of E10.5 mouse embryos using a probe for *Tbx1*. Abbreviations: oe, otic epithelium; nt, neural tube. Blue dashed line outlines the otic epithelium. Top and bottom sections within each embryo cluster ("embryo #1", "embryo #2") are from different levels of the ear in the same embryo. **[n=1 for *Zic2*$^{+/+}$; n=2 for *Zic2*$^{Ku/+}$ and *Zic2*$^{Ku/Ku}$]**

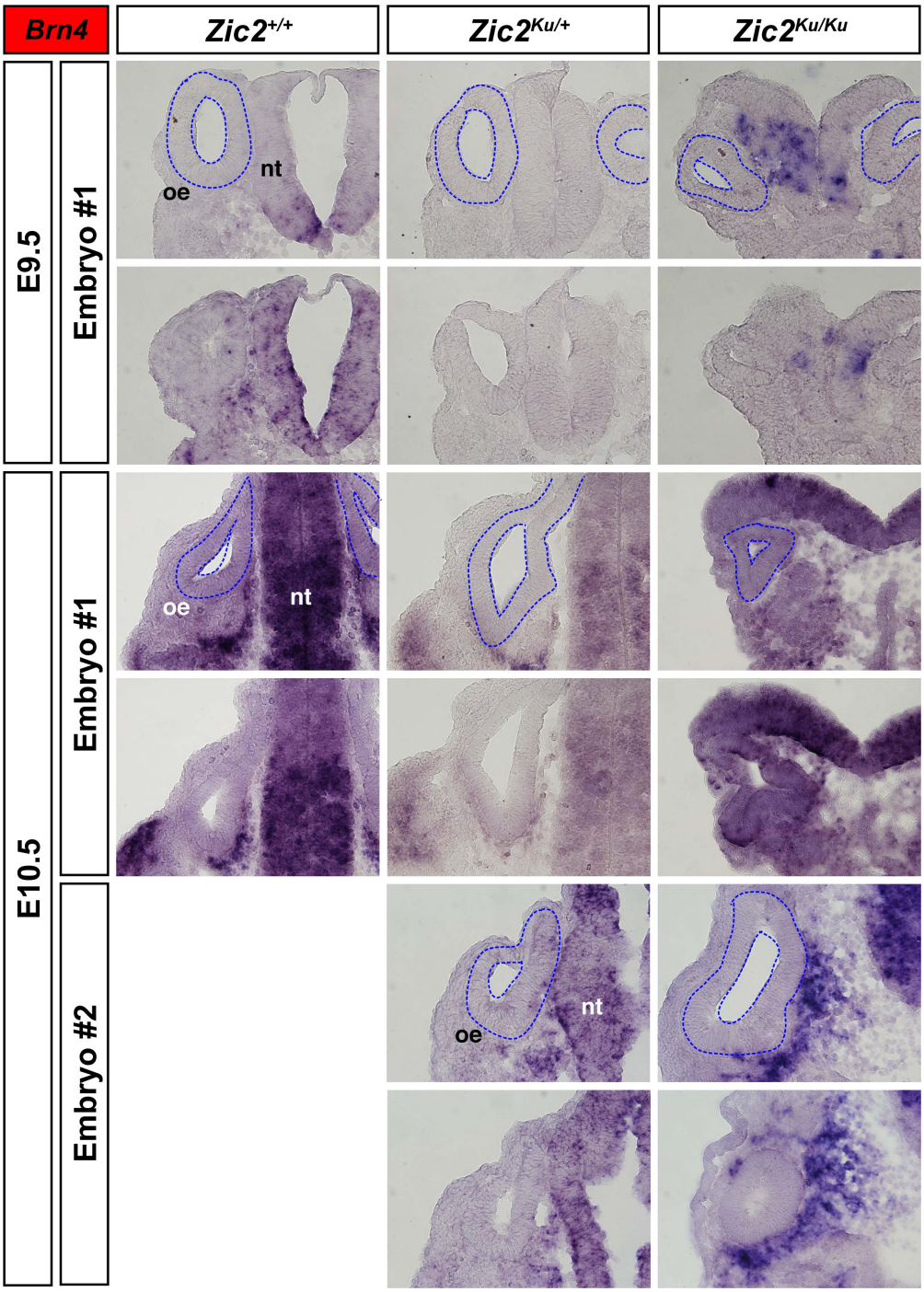

Supplemental Figure 12. *Brn4* expression in the otic region of *Zic2*$^{+/+}$, *Zic2*$^{Ku/+}$, and *Zic2*$^{Ku/Ku}$ mouse embryos at E9.5 and E10.5. *In situ* hybridization on 12µm transverse sections through the otocyst of E9.5 (top 2 rows) and E10.5 (bottom 4 rows) mouse embryos using a probe for *Brn4*. Abbreviations: oe, otic epithelium; nt, neural tube. Blue dashed line outlines the otic epithelium. Top and bottom sections within each embryo cluster ("embryo #1", "embryo #2") are from different levels of the ear in the same embryo. **[E9.5: n=1 for all genotypes; E10.5: n=1 for *Zic2*$^{+/+}$, n=2 for *Zic2*$^{Ku/+}$ and *Zic2*$^{Ku/Ku}$]**

Chapter 4

Future Directions

4.1. Introduction

Work in this thesis demonstrates that *Zic* genes are expressed adjacent to the otic epithelium during inner ear development, and that each of the *Zic* genes (of which there are 5 in the mouse, and 4 in the chicken) has a unique spatiotemporal expression pattern (Chervenak, Hakim et al. 2013). The exact role *Zic* genes play in inner ear development has only begun to be investigated. So far, *Zic2* (Nagai, Aruga et al. 2000; Elms, Siggers et al. 2003) and *Zic1*/*Zic4* (Grinberg, Northrup et al. 2004; Blank, Grinberg et al. 2011) are the only *Zic* genes whose involvement in inner ear development has been studied beyond determining the initial expression pattern. We paint-filled inner ears from $Zic1^{-/-}$;$Zic4^{-/-}$ compound mutants that were sent to us by our collaborator at the University of Washington, Kathy Millen, (Grinberg, Northrup et al. 2004; Blank, Grinberg et al. 2011), but no defects in inner ear morphology were observed. Paint-filled inner ears from $Zic2^{kd/kd}$ embryos (Nagai, Aruga et al. 2000) showed a range of abnormalities in both dorsal (saccule, ED/ES, SCC) and ventral (cochlea) structures, but the molecular mechanism(s) underlying these defects could not be further investigated, as we have not been able to obtain additional fixed tissues from the lab that maintains these mice and which sent us these

original specimens (Jun Aruga, RIKEN). We obtained fixed *Zic2*^{Kumba} mouse embryos (Elms, Siggers et al. 2003) from another collaborator, Ruth Arkell (Australian National University), in whose lab I performed experiments as a visiting student during the Fall 2010 semester. We paint-filled the inner ears at E11.5 and E12.5, the latest time-points available before the embryos die. Inner ears from the *Zic2*$^{Ku/Ku}$ embryos were significantly smaller than those of wild type mice or heterozygotes (Chervenak et al., in preparation for Developmental Dynamics) but had relatively normal morphology at these very early stages of ear development.

To date, we have relied on other labs to supply us with the *Zic2*$^{kd/kd}$, *Zic2*$^{Ku/Ku}$, and *Zic1*$^{-/-}$;*Zic4*$^{-/-}$ embryos. Only very small numbers of fixed embryos were obtainable; breeding schemes in our collaborators' labs were not always successful or timely, and the numbers of embryos available to us at representative stages was rate-limiting. Compounding this, the *Zic2*$^{Ku/Ku}$ mice die before E13.5, which allowed us to study only the earliest phases of inner ear development in the *Zic2*$^{Ku/Ku}$ mutants.

Analysis of *Zic* mutant mice would be among the most direct ways of studying the role of *Zic* genes in inner ear development. However, most of the current *Zic* mutant mouse models show embryonic or perinatal lethality, making it difficult to study all stages of inner ear development (Table 4-1). In addition, *Zic* genes are critical for the development and closure of the neural tube, so mutations often cause neural tube defects, which is especially significant when these defects affect the hindbrain, which is known to affect inner ear